Xu et al. Alzheimer's Research & Therapy (2025) 17:35
https://doi.org/10.1186/s13195-025-01682-1

Alzheimer's Research & Therapy

RESEARCH Open Access

Delta-opioid receptor signaling alleviates neuropathology and cognitive impairment in the mouse model of Alzheimer's disease by regulating microglia homeostasis and inhibiting HMGB1 pathway

Yuan Xu[1,2,3], Naiyuan Shao[1,2], Feng Zhi[1,2], Ronghua Chen[1], Yilin Yang[1,2], Jiahui Li[3,4], Ying Xia[3,4*] and Ya Peng[1,2*]

Abstract

Background Recent studies suggest that opioid receptor signaling may differentially affect Alzheimer's disease (AD) pathology and the relevant behavioral dysfunctions. However, the precise roles and mechanisms of opioid receptor subtypes in AD pathologies are still unclear with major controversies.

Methods We compared the delta-opioid receptor (DOR)- and mu-opioid receptor (MOR)-mediated effects on AD-associated cognitive deficits, pathologies, neuroinflammations, cell death using transgenic APP/PS1 mouse model and BV2 cell line at behavioral, molecular, and cellular levels. Unpaired t-test and one/two way analysis for variance (ANOVA) were used to analyze statistical significance of the data.

Results We show a distinct role of DOR and its major difference with MOR in AD injury in an APP/PS1 mouse model. DOR activation by UFP-512, but not MOR activation by DAMGO, attenuated cognitive impairment, reduced beta-amyloid (Aβ) production and aggregation, as well as protected the neurons from apoptosis in APP/PS1 mice. DOR and MOR also differentially modulated microglia in APP/PS1 mice and in vitro AD cell model with a DOR-mediated inhibition on the excessive activation of microglia and the release of pro-inflammatory cytokines in AD pathologies. Gene expression profiling further revealed that the alternations in DOR/MOR are closely associated with microglial homeostatic signatures and high mobility group protein B1 (HMGB1) in AD. DOR activation inhibited HMGB1 secretion and its translocation from nuclear to cytoplasm. Our in-vitro studies further confirmed that DOR overexpression mitigated microglial inflammatory response and rescued neurons from AD injury via HMGB1-NF-κB signaling pathway.

Conclusions These novel findings uncover previously unappreciated roles of DOR in neuroprotection against AD injury via modulating microglia-related inflammatory responses.

*Correspondence:
Ying Xia
y55738088@gmail.com
Ya Peng
neuropengya@sina.com

Full list of author information is available at the end of the article

Keywords Alzheimer's disease, Cognitive impairment, β-amyloid, Neuroinflammation, Delta-opioid receptor, Microglia, HMGB1.

Introduction

Alzheimer's disease (AD) is the leading cause of dementia, and the incidence is rapidly increasing in aged population in this century [1]. A national cross-sectional study showed that China had roughly 15.07 million people over 60 years old living with dementia, accounting for almost 25% of dementia worldwide [2, 3]. Limited therapeutic approaches have been proven effective in stopping or halting AD progress [1]. A successful strategy for AD therapy should consider both ameliorating the pathological characteristics of this disease and improving the cognitive functional recovery.

AD is characterized by systemic disorders including β-amyloid accumulation, cellular hyper-phosphorylated tau, synapses loss, neuroinflammation and cognitive disability [1, 4]. Opioid receptors have long been considered associated with AD pathology and AD-related behavioral dysfunction [5–7]. Early in 1987, Hiller et al. [8, 9] compared the opioid receptor expression pattern in the brain of age-matched AD patients with the control group and found that the alternations of δ-opioid receptor (DOR) and μ-opioid receptor (MOR) were almost opposite in the caudate nucleus region and hippocampus region of the AD brain, suggesting a potential linkage between opioid receptors and AD. Acetyl choline (ACH), as an important neurotransmitter responsible for learning and memory performance, is majorly regulated by DOR and κ-opioid receptor (KOR), but not MOR [10, 11]. Since the notion "ACH is involved in the pathogenesis of AD" has reached consensus [12], the relationship between opioid receptors and AD became more intriguing.

To date, however, the studies exploring the role of opioid receptors in AD remain sparse and controversial. Two fundamental questions are not answered yet: (1) whether and how opioid receptors are involved in AD pathological events and (2) whether different subtypes of opioid receptors play different roles in AD injury? We addressed these questions genetically and pharmacologically by using Aβ precursor protein/presenilin-1 (APP/PS1) transgenic mice and an in-vitro AD cell model with a focus on the performance of DOR versus MOR in AD. Our novel findings reveal unique and differential roles of DOR vs. MOR in AD pathology and shed light on a potential new target for AD therapy.

Materials and methods

Chemicals and reagents

β-Amyloid (1–42) peptides and DAMGO, a MOR selective agonist were purchased from MCE (Cat: HY-P1388A, HY-P0210, China). UFP-512, a highly specific DOR agonist was synthesized by our research partner [13, 14]. Naltrindole hydrochloride, a selective DOR antagonist, was purchased from Santa Cruz (Cat: sc-202236, USA). Naltrexone hydrochloride, a selective MOR inhibitor was purchase from TOCRIS (Cat: 0677, China). Anti-β-actin antibody, anti-Iba1 antibody, anti-NeuN antibody, anti-Histone H3 antibody, anti-NF-κB antibody, anti-phopho-NF-κB antibody, goat anti-mouse secondary antibody and goat anti-rabbit secondary antibody were purchased from Cell Signaling Technology (Cat: 3700T, 17198 S, 94403 S, 4499T, 8242, 3033, 7076, 7074, USA). Anti- β-amyloid antibody was purchased from Biolegend (Cat: 800708, USA). Anti-DOR antibody, anti-MOR antibody and NF-κB p65 transcription factor assay kit were purchased from Abcam (Cat: ab176324, ab134054, ab133112, USA). CD11b monoclonal antibody, CD45 monoclonal antibody, high mobility group protein B1 (HMGB1) polyclonal antibody, goat anti-Rabbit secondary antibody (Alexa Fluor 594) and goat anti-mouse secondary antibody (Alexa Fluor 594) were purchased from Invitrogen (Cat: 11-0112-82, 14-0451-82, PA1-16926, R37117, R37115, USA). DAPI, Counting Kit-8, one step Terminal deoxynucleotidyl transferase dUTP nick-end labeling (TUNEL) apoptosis assay kit, Immunol staining fix solution, and Human/Mouse/Rat HMGB1 ELISA kit, Nuclear and Cytoplasmic Protein Extraction kit were obtained from Beyotime (Cat: C1006, C0039, C1090/C1086, P0098, PH406, P0028, China). Human/Rat β Amyloid (42) ELISA kit was purchased from Wako (Cat: 292-64501, Japan).

Animals and drug treatment

36 Adult (9-month-old) male APP/PS1 mice and 12 age-matched wild-type mice were purchased from Beijing Viewsolid Biotech Co; Ltd. All the animal work were strictly accordance with the Chinese regulations for the administration of laboratory animals and were approved by the animal ethics committee of Changzhou First People's Hospital. APP/PS1 mice and their wild-type littermates were randomly assigned into 4 groups. APP/PS1 mice were injected intraperitoneally with saline (AD), UFP-512 (1 mg/kg) diluted in saline (AD + U) or DAMGO (1 mg/kg) diluted in saline (AD + D) daily for one week ($n = 12$ per group), respectively. WT mice were injected intraperitoneally with the same volume of saline (WT). UFP-512 and DAMGO were freshly prepared every day during the light cycle. Blind experiments were conducted during behavioral tests. Mice were sacrificed by intraperitoneal injection with 50 mg/kg pentobarbital sodium on the day 14 after drug treatment. The brains

were harvested and dissected into hippocampus and cortex for future applications.

Morris water maze (MWM) test

For spatial learning ability evaluation, MWM test was performed. Briefly, the mice were tested in a circular pool of 90 cm in diameter. The platform (5 cm in diameter) was placed 1 cm above the surface of the water (visible platform phase) or 1 cm below the surface of the water (hidden platform phase). During visible platform phase, mice were pretrained for 2 days, with 4 trials per day, to find the visible platform above the water. During hidden platform phase, the mice were trained for 5 consecutive days, to find hidden platform with 4 trials per day. Each mouse was given 60 s to find the platform. If the animal failed to reach the hidden platform within 60 s, they were guided to the platform and stay there for 15 s. A probe trial was conducted 24 h after the last training. During the probe trial, the platform was removed, and the mice was allowed to swim freely for 60 s. All trials were recorded by video, and the data was analyzed by Animal behavioral test analysis software Smart v3.0. The swimming speed of mice during visible platform test, the escape latency during hidden platform test, the number of mice crossing the platform and the residence time of mice in the target quadrat during probe trial test were recorded.

Novel object recognition (NOR) test

Novel object recognition test was carried out on day 2, 7 and 13 after drug treatment (Fig. 1C). Briefly, the test was divided to habituation phase, familiar phase, and test phase. In the habituation phase, mice were allowed to explore in the empty test chamber for 10 min. In familiar phase, two identical objects were placed in the test chamber. Mice entered the chamber from the location with the same distance to each object and were allowed to explore the objects for 5 min. In the test phase, one familiar object was replaced by a novel one. Animal behavioral test analysis software Smart v3.0 was used to record the activities of mice in the test chamber. The exploration time of mice was limited to 5 min. The number of novel/familiar objects contacting and exploration time for novel/familiar object were recorded to calculate the novel object recognition index (RI).

$$RI = \frac{N}{N+F} \times 100\%$$

N: the exploration time for novel objects/ the number of novel objects contacting.

F: the exploration time for familiar objects/ the number of familiar objects contacting.

Aβ42 measurements

For soluble Aβ42 preparation, the mouse cortex and hippocampus were homogenized in RIPA buffer containing protease inhibitors, respectively. Then the lysate was centrifuged at 15,000 g and the supernatant was collected.

For insoluble Aβ42 preparation, the mouse cortex and hippocampus were homogenized in TBS supplemented with protease inhibitors using a Teflon homogenizer. Subsequently, the lysate was centrifuged at 50,000 g for 20 min. The resulting precipitate was resuspended in TBST containing protease inhibitors, homogenized, and then incubated at 37 ℃ for 15 min. Afterward, a centrifugation at 50,000 g was performed. The precipitate was further incubated with 2% SDS in TBS supplemented with protease inhibitors for 15 min and centrifuge again at 50,000 g. Next, 1 mL of 70% formic acid was added to the precipitate, followed by ultrasonication and centrifugation at 50,000 g at 4℃. The supernatant was collected and dried using a Speed Vac. Finally, the insoluble Aβ42 was harvested and stored in DMSO solvent by ultrasonication.

For measurements of Aβ42, both the soluble and insoluble ones were dissolved in the standard diluent. Their levels were determined using a Human/Rat β Amyloid (42) ELISA kit. The details of Aβ42 measurement have been described previously [15]. The absorbance was read at 450 nm with a multi-well microplate reader.

Immunohistochemical/immunofluorescence staining

The harvested brains were fixed in 4% paraformaldehyde and embedded in paraffin at 58 ℃. The embedded tissue was then cut into 10-μm-thick tissue sections, which was floated in a 56 ℃ water bath. The sections were mounted onto gelatin-coated histological slides and stored at room temperature overnight. Before staining, heat-induced antigen retrieval was performed using antigen retrieval buffer. To quench endogenous peroxidase activity, brain sections were pretreated with 3% H_2O_2 for 10 min, and then rinse in wash buffer for 5 min. Subsequently, the slides were blocked with serum blocking reagent, avidin blocking reagent, and biotin blocking reagent each for 15 min. The sections were then incubated with anti-amyloid plaques (1:5000), anti-NeuN (1:2000), anti-HMGB1 (1:200) and anti-Iba1 (1:200) overnight at 4℃. After three-times washes with wash buffer, the sections were incubated with secondary antibody (1:2000) for 1 h at room temperature and rinsed for another 3 times. For immunohistochemical staining, the samples underwent a 30-mins incubation with HRP and incubation with DAB/AEC chromogen (not required for immunofluorescent staining). The stained tissue was visualized under microscope. The plaque number, HMGB1 positive cells or Iba1 positive cells were calculated from at least 3 randomly selected microscopic fields of each section.

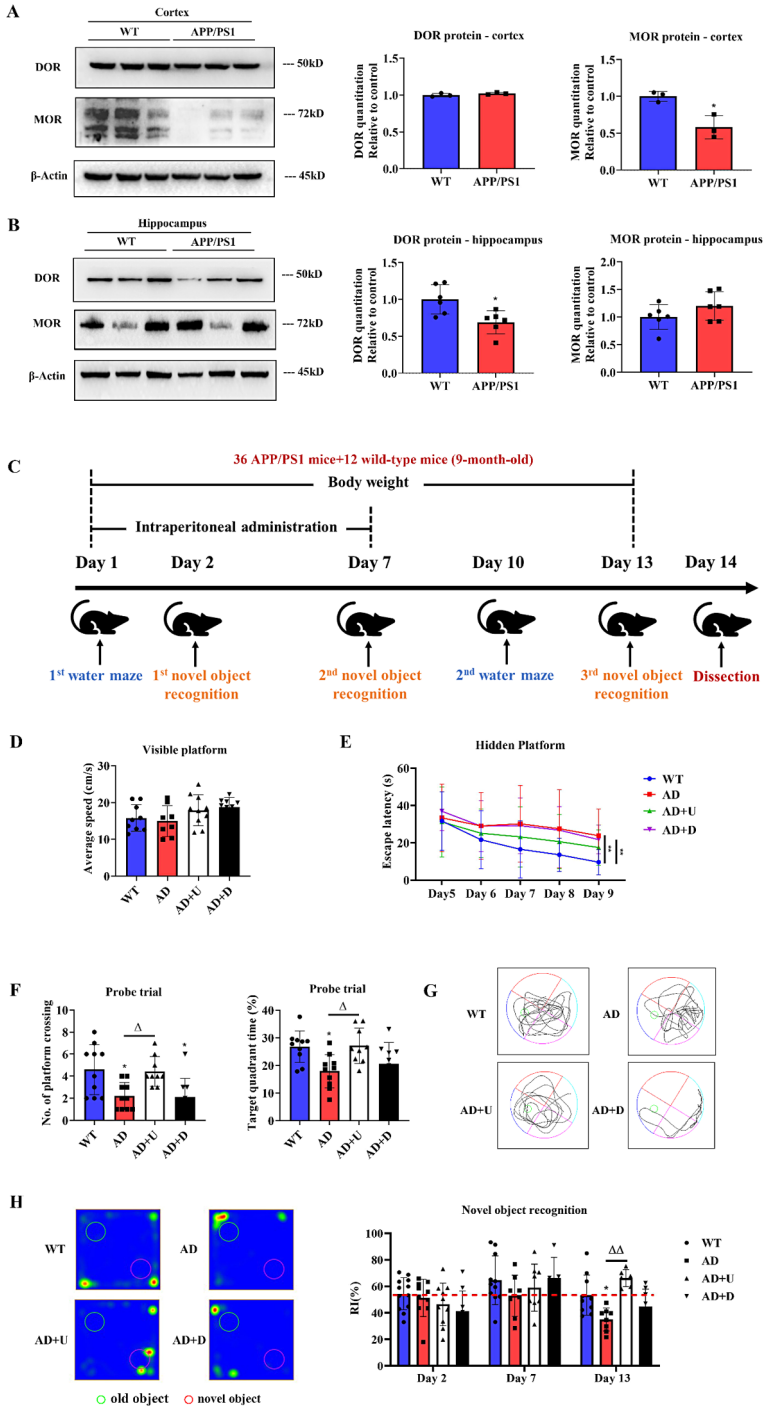

Fig. 1 DOR activation improved cognitive performance of APP/PS1 mice. WT: wild type C57 mice treated with saline intraperitoneally; AD: APP/PS1 mice treated with saline intraperitoneally; AD + U: APP/PS1 mice treated with UFP-512 intraperitoneally; AD + D: APP/PS1 mice treated with DAMGO intraperitoneally. (**A**),(**B**) Expression profile of DOR and MOR in the cortex and hippocampus region of WT mice and AD mice. $n = 3$ in cortex; $n = 6$ in hippocampus, MOR: $^{*}p = 0.0136$ vs. WT in Fig. 1A; DOR: $^{*}p = 0.013$ vs. WT in Fig. 1B. Unpaired t-test was used to analyze the statistical significance in Fig. 1A and B. (**C**) Schematic diagram of mice treatment and behavioral tests. (**D-G**) Effects of DOR and MOR on spatial learning and memory evaluated by MWM. $n = 10$. One-way ANOVA was used to analyze the statistical significance in Fig. 1D and F. Two-way ANOVA was used to analyze the statistical significance in Fig. 1E. **(D)** The swimming speed was recorded during visible platform tests. (**E**) Escape latency during hidden platform tests was recorded every training day. $^{**}p < 0.0012$ or 0.0014 vs. WT. (**F**) A probe trial was performed on Day 10. The number of mice crossing the previous platform located quadrant and the time mice spent in the target quadrant were recorded. Left panel: $^{*}p = 0.0160$ or 0.0148 vs. WT; $^{\Delta}p = 0.0322$ vs. AD. Right panel: $^{*}p = 0.0207$ vs. WT; $^{\Delta}p = 0.0189$ vs. AD. (**G**) Representative trajectory chart of mice in MWM test. (**H**) Effects of DOR and MOR on mice recognitive abilities evaluated by NOR. $n = 10$. Day 13: $^{*}p = 0.0479$ vs. WT; $^{\Delta\Delta}p = 0.0011$ vs. AD. Two-way ANOVA was used to analyze the statistical significance in Fig. 1H

TUNEL assay

Apoptosis cells were detected by one step TUNEL apoptosis assay kit from Beyotime according to the manufacturer's instructions. Briefly, the slides were fixed using Immunol staining fix solution and then permeated in PBS containing 0.3% Triton X-100. After two times washing with PBS, slides were incubated with TUNEL detection solution for 60 min at 37 ℃. After DAPI staining, the slides were visualized under microscope at 550 nm wavelength.

mRNA quantification

To measure the changes in the target mRNA, total RNA was extracted and purified using Trizol reagent following the RNA extraction instruction. The extracted RNA (1 μg) was used as the template to generate cDNA. RT-PCR (Applied Biosystems, USA) was performed to quantify the mRNA relative content. The primers designed are listed as below, and the primers were synthesized by Genscript Co., China.

TNF-α mRNA primers	F: 5′CAAGGGACAAGGCTG CCCCG 3′	R: 5′GCAGGGGCT CTTGACGGCAG 3′
IL-1β mRNA primers	F: 5′AAGCCTCGTGCTGTCG GACC 3′	R: 5′TGAGGCCCA AGGCCACAGG 3′
iNOS mRNA primers	F: 5′CAGCTGGGCTGTACAA ACCTT 3′	R: 5′CATTGGAAGT GAAGCGTTTCG 3′
GAPDH mRNA primers	F: 5′GCCAAGGCTGTGGGC AAGGT 3′	R: 5′TCTCCAGGCG GCACGTCAGA 3′
DOR mRNA primers	F: 5′CCATCACCGCGCTCT ACTC 3′	R: 5′GTACTTGGCG CTCTGGAAGG 3′
MOR mRNA primers	F: 5′CCAGGGAACATCAGC GACTG 3′	R: 5′GTTGCCATCA ACGTGGGAC 3′

Flow cytometric analysis

The mouse brain tissue was chopped into small particles in ice-cold PBS supplemented with 0.3% BSA and incubated with 10 ml of digestion buffer for 1 h at 37 ℃. The resulting suspension was filtered through a 70 μm cell strainer. After centrifuge at 400 g for 10 min, the pellet was resuspended in PBS for washing and then collected in PBS containing 0.3% BSA. The suspension was stained with anti-mouse-CD45-APC (1 ug/test) and anti-mouse CD11b-FITC (0.5 ug/test) to assess the cerebral infiltration of microglia and macrophages ($CD11B^{+}CD45^{int-high}$ cells). Flow cytometric analysis was carried out by using FlowJo. The first gate was defined in the dot plot Forward-Scattered-Area (FSC-A) versus Forward-Scattered-Height (FSC-H) to distinguish single cells from doublets (Supplementary 1 A). The single cells were then gated on FSC-A versus Side-Scattered-Area (SSC-A) dot plots based on the relative cell size and cell granularity (Supplementary 1B) [16]. Then the microglia and the macrophages were identified based on their expression levels of CD11b/CD45 markers (Supplementary 1 C).

Cell cultures and treatments

Mouse BV2 cell line (a commonly used microglia) was obtained from National Infrastructure of Cell Line Resource (NICR), Beijing, China (Cat: 1101MOU-PUMC000063). The HT22 cell line (hippocampal neuron) was purchased from the Type Culture Collection of the Chinese Academy of Sciences, Shanghai, China. Both BV2 cells and HT22 cells were cultured in DMEM containing 10% FBS. BV2 cells were randomly subjected to normal condition, and Aβ1-42 oligomer exposure. DOR specific agonist UFP-512 (5 μM), DOR antagonist naltrindole (1 μM), MOR agonist DAMGO (5 μM) or MOR selective antagonist naltrexone (5 μM) were used to treat BV2 cells for 48 h as we previously described [15, 17].

Aβ1-42 oligomer preparation

Aβ1-42 oligomers were prepared following the methods described in our prior work and other studies [18–20]. Briefly, 1 mg of Aβ1-42 peptide was dissolved in 222 μl hexafluoroisopropanol (HFIP) and then aliquoted into sterile tubes, with 55 μl per tube. A speed Vacuum was employed to evaporate the HFIP, yielding a colorless and transparent Aβ1-42 peptide film. The film was stored at -20 ℃ until further use. For oligomer applications, DMSO was added to the film, followed by sonication in a water bath with a power of 300 W and a frequency of 35 Hz for 10 min. Subsequently, 539 μl of pre-cooled PBS was added to the Aβ-DMSO solution to achieve a final concentration of 100 μM. Typically, the prepared solution was incubated at 37 ℃ for 24 h to facilitate oligomer formation. The vehicle was prepared in the same way, except without Aβ addition.

Nuclear and cytoplasmic protein extraction

For cytoplasmic and nuclear protein extraction, the Nuclear and Cytoplasmic Protein Extraction Kit was used to isolate the nuclear and cytoplasmic fractions. Firstly, the cells were rinsed with pre-cooled PBS and then harvested using a cell scraper. After centrifugation, the cell pellet was resuspended in cytoplasmic isolation reagent A supplemented with PMSF and vortexed for 5 s. After 15 min incubation on ice, cytoplasmic isolation reagent B was added to the cells, which was then centrifuged at 12,000 g for 5 min. The resulting supernatant obtained was cytoplasmic protein. For nuclear protein extraction, the pellet was further diluted in nuclear isolation reagent containing PMSF. The solution was vortexed for 20 s and homogenized on ice for 2 min. The cycle was repeated for 30 min. Subsequently, the cell suspension was centrifuged at 12,000 g for 10 min at 4℃. The supernatant was collected as the nuclear fraction.

Co-culture of neurons and microglia

HT22 cells were plated on 12-well plates, and microglia BV2 cells were seeded in the transwell inserts for indirect co-culture model study of neuron-microglia crosstalk. The BV2 cells, HT22 cells were grown in a 1:5 (microglia: neuron) ratio. Both BV2 cells and HT22 cells were cultured in DMEM containing 10% FBS and were exposed to 20 μM Aβ1-42 oligomer the second day for 48 h. ELISA was used to measure the HMGB1 contents in the supernatant. Western blot was used to quantify HMGB1 expression in the HT22 cells. Q-PCR analysis was used to study the mRNA expressions of cytokines in neurons. Immunofluorescence staining and CCK8 were used to study cell apoptosis.

Cell viability assay

Cell viability was assessed using the CCK8 kit. Exponentially growing BV2 cells and HT22 cells were seeded in co-culture system as we described above. Blank control was established. After 48 h of drug treatment, the original medium was removed. Subsequently, 500 μl of fresh culture medium was added to each well, following by 50 ul of CCK8 reagent. The cells were incubated with CCK8 reagent for 2 h and the absorbance was measured at a wavelength of 450 nm with a microplate reader (Biotek, VT, USA).

Western blot

The details of Western blot protocol were described in our previous work [15, 17]. In brief, cells or tissues were lysed using the lysis buffer containing 0.5% 100 mM PMSF, 0.1% protease inhibitor, and 1% phosphatase inhibitor. 40 ug of protein samples were run in 10-12.5% SDS-PAGE electrophoresis and transferred to hydrophobic polyvinylidenedifluorid (PVDF) membranes. The membranes were then blocked by TBST with 5% milk or TBST with 5% BSA, and then incubated with certain primary antibodies (1:1000 in general). HRP conjugated secondary antibodies (1:2000 in general) were used to detect specific protein expression. The binding of antibody was detected by chemiluminescence using Western Lightening® Chemiluminescence Reagent Plus (Perkin-Elmer, USA). The data was analyzed using the NIH Image program (Image J).

NF-κB p65 DNA-binding activity assay

The cell nuclei of cortical and hippocampal tissues were extracted with the Nuclear and cytoplasmic protein extraction kit following the manufacturer's instructions. A small portion of the nuclear extract was retained to quantify the protein concentration, and the remainder was used for subsequent tests. For binding activity measurement, in a 96-well plate, 90 μL of Complete Transcription Factor Binding Assay Buffer (CTFB) was added, followed by 10 μL of nuclear extract as the sample wells. Positive control wells (PC) and non-specific binding wells (NSB) were also set. After overnight incubation at 4 °C, the wells were emptied, and each well was washed with 200 μL of wash buffer. The transcription factor NF-κB primary antibody and secondary HRP conjugate antibody were then added, followed by carefully washes after each antibody addition. Finally, 100 μL of transcription factor developing solution and 100 μL of stop solution were successively added to each well. The absorbance at 450 nm was measured and the data were recorded.

Lentivirus infection

The lentiviral plasmids capable of knocking down DOR, overexpressing DOR or overexpressing MOR were obtained from GENECHEM, Shanghai, China. For knocking down or overexpressing DOR, the negative control-NC207 was set. For overexpressing MOR, the negative control-NC794 was set. BV2 cells were seeded in a 6- well plate at the concentrations of 2×10^5 cells per well and incubated overnight. HiTransG A was added with lentiviral plasmids in 10% FBS DMEM to enhance the infection efficiency (MOI = 20). After 16-hrs incubation, the medium containing the plasmids and HiTransG A was removed, and the infected cells were cultured in fresh medium for 48 h. 4 μg/ml puromycin was employed to screen the infected cells for an addition 48 h. PCR and western blotting were utilized to assess the expression level of DOR and MOR.

RNA-seq and analysis

Total RNA of the hippocampus and cortex was extracted from mouse brains, or BV2 cell line using Trizol reagent kit. RNA quality was assessed on an Agilent 2100 Bioanalyzer (Agilent Technologies, Palo Alto, CA, USA) and checked using RNase free agarose gel electrophoresis. After total RNA was extracted, eukaryotic mRNA was enriched by Oligo(dT) beads. Then the enriched mRNA was fragmented into short fragments using fragmentation buffer and reversely transcribed into cDNA by using NEBNext Ultra RNA Library Prep Kit for Illumina (NEB #7530, New England Biolabs, Ipswich, MA, USA). The purified double-stranded cDNA fragments were end repaired, A base added and ligated to Illumina sequencing adapters. The ligation reaction was purified with the AMPure XP Beads (1.0X). Ligated fragments were subjected to size selection by agarose gel electrophoresis and polymerase chain reaction (PCR) amplified. The resulting cDNA library was sequenced on the Illumina sequencing platform by 10 K Geonomics, Shanghai, China.

RNAs differential expression analysis was performed by DESeq2 software between two different group [21]. The genes/transcripts with the parameter of false discovery rate (FDR) below 0.05 and absolute fold change ≥ 2 were

considered differentially expressed genes/transcripts. After that, Venn diagram was generated by Venny 2.1 online tool (https://bioinfogp.cnb.csic.es/tools/venny/index.html), enrichment analyses were based on the KEGG pathway (https://www.genome.jp/kegg/pathway.html).

HMGB1 release measurement

In accordance with the instruction of Human/Mouse/Rat HMGB1 ELISA kit, the supernatant of cultured cells was harvested and centrifuged at 500 g for 5 min to eliminate cell debris. Subsequently, 100 μL of the supernatant and 100 μL of standards were separately added to the wells and incubated at room temperature for 2 h. After five washes, 100 μL of HRP-labeled HMGB1 antibody was introduced to the plate, followed by an additional 1 h incubation at room temperature. The plate was washed prior to each reagent addition step. Then, 100 μL of HRP-labeled Streptavidin were added to each well and incubated in the dark for 20 min. Finally, TMB solution was added to initiate the HRP reaction in the dark. Once the reaction was terminated by stop solution, the absorbance was read at 450 nm with a multi-well microplate reader.

Statistical analysis

All data are presented as means ± SD. Each independent experiment was performed at least three times. The number (n) of conducted experiments is indicated in figure captions. Unpaired t-test, one-way analysis for variance (ANOVA) followed by Bonferroni's multiple comparison tests and two-way ANOVA were used to analyze statistical significance in our work (Prism 5, GraphPad Software, CA, USA).

Results

DOR and MOR proteins decreased in different regions of APP/PS1 transgenic mice

Altered DOR and MOR expressions have been observed in several cerebral disorders in vivo and in vitro [17, 22–24]. However, it is still unclear whether opioid receptors are altered in AD pathological process. We therefore examined the expression level of DOR and MOR, two major subtypes of opioid receptors, in the cortical and hippocampal regions of APP/PS1 mice. In 9-month-old APP/PS1 mice, MOR protein in the cortex significantly decreased ($^{*}p < 0.05$, Fig. 1A), but the level of DOR protein had no appreciable change in the same region between APP/PS1 mice and WT mice (Fig. 1A). In the hippocampal region, APP/PS1 mice presented a slight decrease in DOR protein ($^{*}p < 0.05$, Fig. 1B) with an unappreciable increase in MOR protein (Fig. 1B) as compared to WT mice. Consistent with the Western blot data, MOR also showed a decrease in cortical region with a red fluorescent ($^{**}p < 0.01$, Supplementary 2 A, 2B), while the density of DOR decreased in the hippocampus with a green fluorescent in the APP/PS1 mouse brain slices stained with MOR (red), DOR (green) and DAPI (blue) ($^{***}p < 0.001$, Supplementary 2 A, 2B). The different changes in DOR and MOR expression raise the possibility of their differential roles in AD pathology.

DOR activation reversed cognitive impairments in APP/PS1 mice

To clarify the role of DOR or MOR in AD, 36 APP/PS1 mice (9-month-old) and their 12 wild-type littermates were randomly allocated to 4 groups (12 mice per group). APP/PS1 mice were injected intraperitoneally with saline (AD), UFP-512 (1 mg/kg diluted in saline) which specifically activate DOR (AD + U) or DAMGO (1 mg/kg diluted in saline) which selectively activate MOR (AD + D) daily for one week, respectively. WT mice were injected intraperitoneally with the same volume of saline (WT) compared to APP/PS1 mice. All these mice were subjected to MWM training and NOR training as Fig. 1C showed. In MWM test, we did not see any appreciable change in average speed between APP/PS1 and WT mice during the visible platform training (Fig. 1D), suggesting a minimal difference in swimming ability between APP/PS1 and WT mice. Notably, during the hidden platform training, APP/PS1 mice exhibited a significantly prolonged escape latency compared with WT ($^{**}p < 0.01$ vs. WT, Fig. 1E). UFP-512 treatment shortened the escape latency of APP/PS1 mice, while DAMGO did not show any evident benefits on the escape latency of APP/PS1 mice ($^{**}p < 0.01$ vs. WT, Fig. 1E). We performed probe trial tests on Day 1 and Day 10 as the schedule in Fig. 1C depicted. During the test, both the number of crossings over the previous platform location and the time spent in the previous target quadrant of APP/PS1 mice were badly disturbed compared to WT mice ($^{**}p < 0.01$, $^{*}p < 0.05$ vs. WT, Fig. 1F and G, Supplementary 2 C) within the studied period. UFP-512 effectively improved the spatial cognitive performances of APP/PS1 mice on Day 10, which was close to the normal level of WT mice ($^{\Delta}p < 0.05$ vs. AD, Fig. 1F and G). In sharp contrast, DAMGO failed to ameliorate the cognitive impairments in APP/PS1 mice in Day 10 MWM tests as shown in Fig. 1F.

We also conducted NOR tests to further verify the effectiveness of UFP-512 in improving learning and memory abilities in APP/PS1 mice. As depicted in Fig. 1H, On Day 2, 7, and 13, APP/PS1 mice showed a decrease in recognitive index especially on Day 13 ($^{*}p < 0.05$ vs. WT, Fig. 1H). UFP-512 treatment increased the tendency of APP/PS1 mice to interact with novel object, and this effect is more evident in Day 13 test ($^{\Delta\Delta}p < 0.01$ vs. AD, Fig. 1H). DAMGO treatment tended to improve recognitive index of APP/PS1 mice on Day 7 but with a major reduction in recognitive index in the Day 13-test.

All these results suggest that DOR, but not MOR activation, is more effective in attenuating cognitive impairment in APP/PS1 mice.

DOR activation reduced Aβ production and aggregation in APP/PS1 mice

We have previously demonstrated, in both Aβ1-42 oligomer treated highly differentiated PC12 cell line and APP mutant (APPswe) SH-SY5Y cell line, that DOR and MOR played almost opposite role in β-site APP cleaving enzyme 1 (BACE1) regulation, with DOR activation significantly attenuated BACE1 expression and activity, thus contributing to decreased Aβ production [15]. In this work, we further evaluated the effects of DOR and MOR on AD-like pathologic changes in APP/PS1 mice. Firstly, we examined the alternations of soluble and insoluble Aβ peptides in the cortex and hippocampus of APP/PS1 mice by using β amyloid (42) ELISA kit. As shown in Fig. 2A, the contents of soluble and insoluble Aβ42 were sharply increased in APP/PS1 mice both in the cortical and hippocampal regions ($^{*}p<0.05$, $^{***}p<0.001$, $^{****}p<0.0001$ vs. WT, Fig. 2A). DOR activation with UFP-512 effectively decreased insoluble Aβ42 in hippocampus ($^{\Delta\Delta}p<0.01$, vs. AD, Fig. 2A). Moreover, we observed a tendency of reduction in insoluble Aβ42 in the cortex of APP/PS1 mice treated with UPF-512 although not reaching to a statistically significance. Unexpectedly, the soluble Aβ42 in the hippocampus of DAMGO-treated mice also showed a remarkable decrease compared to APP/PS1 mice treated with saline ($^{\Delta\Delta}p<0.01$, vs. AD, Fig. 2A). DAMGO treatment did not effectively alter soluble Aβ42 level in the cortex, and insoluble Aβ42 at all both in the cortex and hippocampus of APP/PS1 mice.

We then measured the effects of DOR and MOR on Aβ plaques by immunohistochemical technique. As Fig. 2B depicted, massive Aβ plaques were distributed in the cortex and hippocampus of APP/PS1 mice, while the plaques were undetectable in WT mice ($^{***}p<0.001$, vs. WT, Fig. 2B). DOR agonist UFP-512 administration reduced Aβ plaques in both quantity and volume in AD mouse model. The number of Aβ plaques in UFP-512 treated APP/PS1 mice decreased about 39.7% compared to saline-treated APP/PS1 mice (Fig. 2B). The

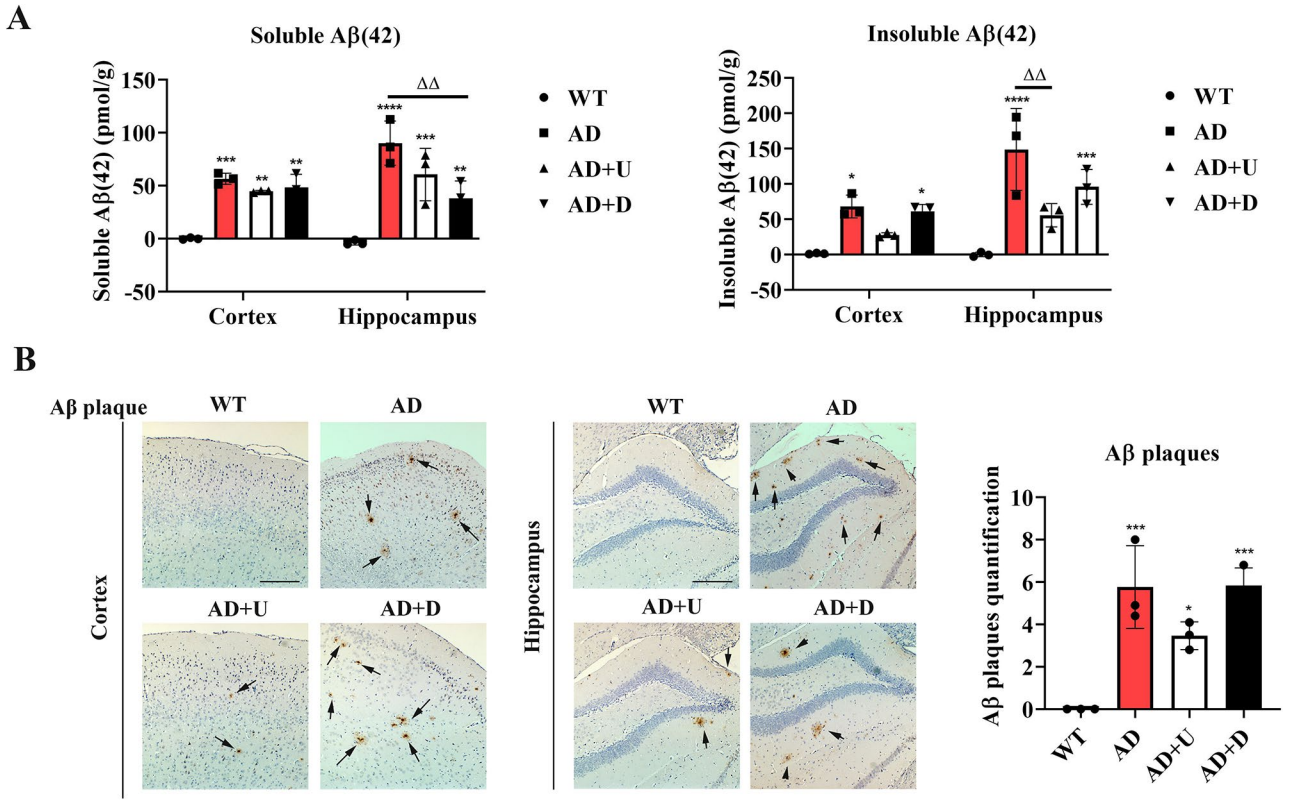

Fig. 2 DOR activation attenuated Aβ generation and aggregation both in the cortex and hippocampus of APP/PS1 mice. (**A**) Effects of DOR and MOR on the level of soluble and insoluble Aβ42 in the cortex and hippocampus of APP/PS1 mouse brains. $n=3$. Left panel: Cortex: $^{***}p=0.0006$, $^{**}p=0.0053$ or 0.0026 vs. WT. Hippocampus: $^{****}p<0.0001$, $^{***}p=0.0002$, $^{**}p=0.0091$ vs. WT; $^{\Delta\Delta}p=0.0014$ vs. AD. Right panel: Cortex: $^{*}p=0.0174$ or 0.0345 vs. WT. Hippocampus: $^{*****}p<0.0001$, $^{***}p=0.0009$ vs. WT; $^{\Delta\Delta}p=0.0011$ vs. AD. Two-way ANOVA was used to analyze the statistical significance. (**B**) Effects of DOR and MOR on the Aβ-positive plaques number in the cortex and hippocampus. $n=3$ mice per group for statistical analysis. Scale bar = 100 μm in panel. $^{*}p=0.0211$, $^{***}p=0.001$ or 0.0009 vs. WT. One-way ANOVA was used to analyze statistical significance

administration of MOR agonist DAMGO had no appreciable effect on Aβ plaques in APP/PS1 mouse brain.

These data reveal the inhibitory effect of DOR activation on Aβ aggregation in APP/PS1 mice with differential effects of MOR activation on the same targets.

DOR activation corrected gene expression abnormality and rescued neuronal apoptosis in the APP/PS1 mice

To explore the cellular and molecular underpinnings linking DOR/MOR treatment with AD symptomatic and pathologic improvement, we conducted RNA-seq analysis of AD models with and without UFP-512/DAMGO treatment (Fig. 3A and B). We collected brain tissue from 9-month aged WT and APP/PS1 mice treated with either UFP-512 or DAMGO. Each group included three mice. The cortex and hippocampus from each brain were dissected and sequenced separately. The expression profiles of APP/PS1 mice showed substantial changes compared to WT both in the cortex and hippocampus regions (Fig. 3A). In contrast, many fewer differentially expressed genes (DEGs) were present in the comparison of UFP-512-treated APP/PS1 samples with the WT samples (Fig. 3A). Indeed, 75% and 67.17% of expression changes in the cortex and hippocampus of APP/PS1 mice were corrected by UFP-512 treatment (Fig. 3B, left panel), while only 18.5% and 5.99% of the expression changes of APP/PS1 samples were corrected by MOR agonist DAMGO, respectively (Fig. 3B). The list of all UFP-512-correted DEGs in the cortex and hippocampus was analyzed for pathway enrichment with Kyoto Encyclopedia of Genes and Genomes (KEGG) (Supplementary 3). Specifically, UFP-512-corrected DEGs were strongly related to complement cascade, Alzheimer's disease, and immune response (Supplementary 3).

Additionally, TUNEL staining was used to evaluate neuronal injury after UFP-512/ DAMGO treatment in the APP/PS1 mice. Compared with the WT group, TUNEL-positive apoptotic cells were significantly increased in APP/PS1 mice ($^{****}p < 0.0001$ vs. WT, Fig. 3C). Notably, DOR agonist UFP-512 remarkably reduced TUNEL-positive cells and the TUNEL fluorescence intensity in cortex, CA1 and DG regions of APP/PS1 mice ($^{\Delta\Delta\Delta}p < 0.001$ vs. AD, Fig. 3C), while MOR agonist DAMGO did not seriously change TUNEL staining in APP/PS1 mice. Consistently, we also found that UFP-512 mildly restored neuronal number as calculated by $NeuN^+/DAPI^+$ cells in the APP/PS1 mouse brain (Fig. 3C).

Taken together, these results indicate that activating DOR using UFP-512 induced protective effects at cellular and molecular levels in AD mouse model.

DOR activation inhibited neuroinflammatory events in APP/PS1 mouse brain and AD-mimicked BV2 cells

Since neuroinflammation is implicated in the pathogenesis of AD [25], we performed qPCR to evaluate the inflammatory events in APP/PS1 mice. Firstly, we measured the mRNA levels of several key molecules for pro-inflammation including TNF-α, IL-1β and inducible nitric oxide synthase (iNOS), in APP/PS1 mice as compared to those of WT mice. We found that APP/PS1 mice exhibited a significant increase in TNF-α and IL-1β release both in the cortex region and hippocampus region compared to the WT mice ($^{*}p < 0.05$, $^{**}p < 0.01$, vs. WT, Fig. 4A). Since iNOS, though tend to increase, did not show a significant increase, we chose TNF-α and IL-1β as the measuring indexes in our subsequent experiments. As Fig. 4B and C presented, DOR activation with UFP-512 effectively inhibited the release of TNF-α and IL-1β ($^{\Delta}p < 0.05$, vs. AD, Fig. 4B and C), while MOR activation did not have such effect, neither in the cortex and hippocampus of APP/PS1 mice. These data suggest that DOR activation, but not MOR activation, exhibits strong capacity to fight against neuroinflammation in the brain of APP/PS1 mice.

Microglia is the major immune cell type in the CNS acting as the monitor of the native immune microenvironment and the regulator of neuroinflammation [25]. Since UFP-512-correted DEGs were closely associated with immune response, we asked if DOR activation inhibited neuroinflammation and protected APP/PS1 mouse brain through its effects on microglia. We chose BV2 cell line to establish the in vitro AD model by treating BV2 cells with 5–20 μM Aβ1-42 oligomer. Firstly, we found that the increased concentration of Aβ1-42 oligomer gradually reduced DOR density in BV2 cell line which was evident when 20 μM of Aβ1-42 oligomer was applied ($^{**}p < 0.01$, vs. C, Supplementary 4 A), while MOR was not seriously affected by Aβ1-42 induced AD injury (Supplementary 4B). Furthermore, qPCR results showed that Aβ1-42 oligomer led to a significant increase in TNF-α and IL-1β in BV2 cell line ($^{*}p < 0.05$, $^{**}p < 0.01$, $^{***}p < 0.001$, $^{****}p < 0.0001$ vs. C, Fig. 4D), but did not significantly increase iNOS, which is consistent with our observations in APP/PS1 mice. Given that, we continued to treat BV2 cells with DOR agonist UFP-512, DOR antagonist naltrindole, MOR agonist DAMGO, or MOR antagonist naltrexone respectively. Although both UFP-512 and naltrindole did not alter DOR expression in BV2 cells exposed to 20 μM Aβ1-42 oligomer (Supplementary 4 C), the administration of UFP-512 effectively attenuated the Aβ1-42 oligomer induced release of TNF-α and IL-1β ($^{\Delta\Delta}p < 0.01$, vs. A, Fig. 4E). The antagonism of DOR totally abolished this effect. In contrast, MOR activation or inhibition did not significantly change MOR density in

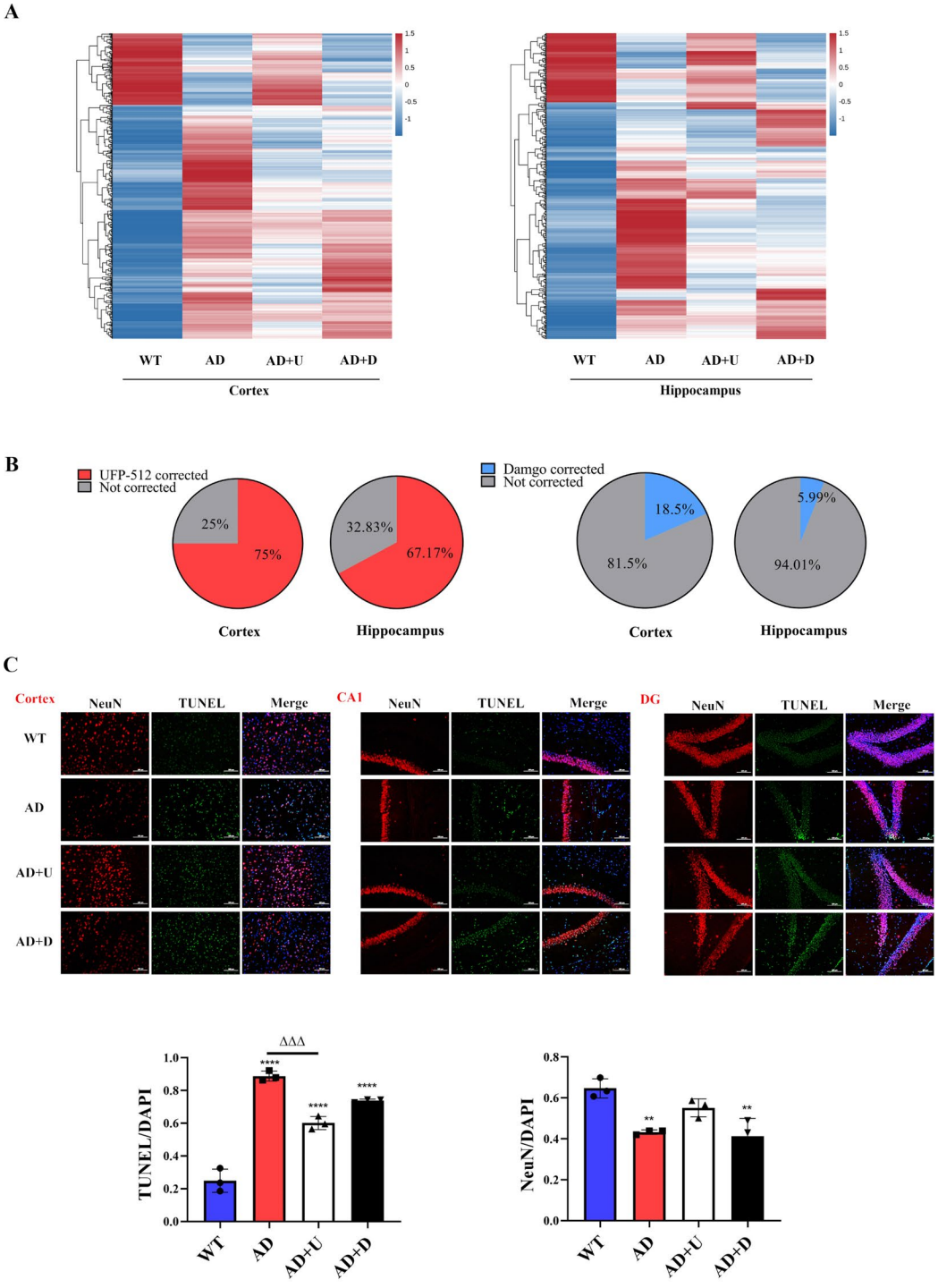

Fig. 3 DOR or MOR-mediated regulation of gene expression profiles and anti-apoptosis in AD mouse model. (**A**)(**B**) DEGs in the cortex and hippocampus of WT, AD, AD + U and AD + D mice. Heatmaps show representative single DEG expression within each group. Pie charts illustrate percentage of DEGs which are corrected by UFP-512 treatment or DAMGO treatment. $n = 3$. UFP-512 corrected p value = 0.0172 in cortex, while UFP-512 corrected p value = 0.6718 in hippocampus. DAMGO corrected p value = 0.3187 in cortex, while DAMGO corrected p value = 0.046 in hippocampus. Chi-square test was used to analyze the statistical significance. (**C**) Representative images of TUNEL staining and NeuN staining, together with quantification of TUNEL-positive cells and neuronal proportion in the cortex and hippocampus of APP/PS1 mice. $n = 3$ mice per group for statistical analysis. Scale bar = 100 μm in panel. Left panel: $^{****}p < 0.0001$ vs. WT; $^{\Delta\Delta\Delta}p = 0.0002$ vs. AD. Right panel: $^{**}p = 0.0057$ or 0.0033 vs. WT. One-way ANOVA was used to analyze statistical significance

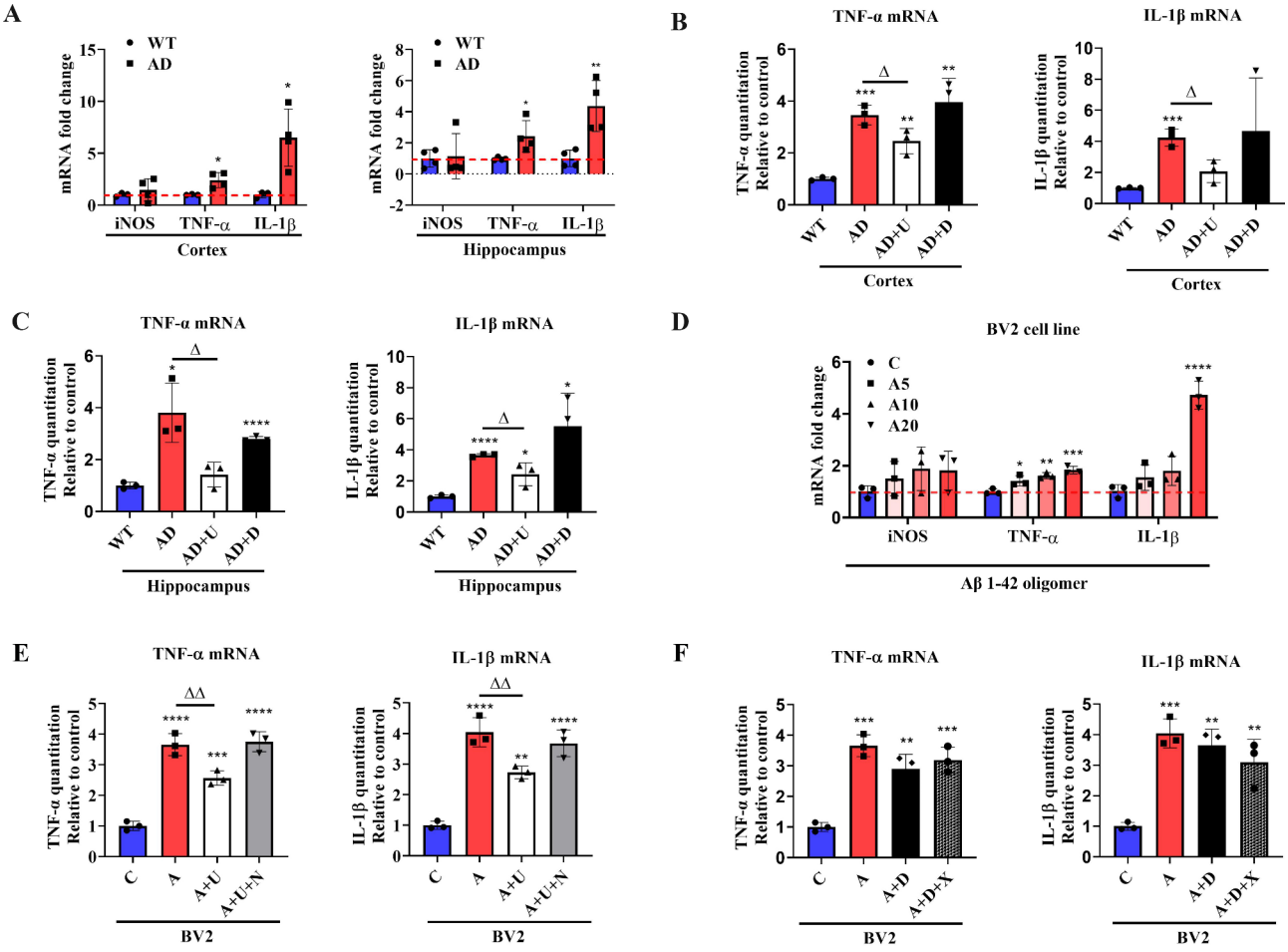

Fig. 4 DOR activation inhibited inflammatory cytokines release in APP/PS1 mouse and Aβ1-42 oligomer exposed BV2 cell line. C: the control BV2 cells; A: Aβ1-42 oligomer exposed BV2 cells; U: UFP-512; N: naltrindole; D: DAMGO; X: naltrexone. (**A**) Evaluation of the inflammatory events in the cortex and hippocampus region of WT mice and APP/PS1 mice. $n=4$. Cortex: TNF-α: $^{*}p=0.0218$ vs. WT. IL-1β: $^{*}p=0.0203$ vs. WT. Hippocampus: TNF-α: $^{*}p=0.0286$ vs. WT. IL-1β: $^{**}p=0.0080$ vs. WT. Unpaired t test was used to analyze the statistical significance. (**B**,**C**)Effects of DOR and MOR on inflammatory cytokines in the cortex and hippocampus of APP/PS1 mice. $n=3$. Cortex: TNF-α: $^{***}p=0.0004$, $^{**}p=0.0068$ or 0.0050 vs. WT; $^{\Delta}p=0.0477$ vs. AD. IL-1β: $^{***}p=0.0005$ vs. WT; $^{\Delta}p=0.0149$ vs. AD. Hippocampus: TNF-α: $^{****}p<0.0001$, $^{*}p=0.0133$ vs. WT; $^{\Delta}p=0.0288$ vs. AD. IL-1β: $^{****}p<0.0001$, $^{*}p=0.0291$ or 0.0217 vs. WT; $^{\Delta}p=0.0467$ vs. AD. Unpaired t test was used to analyze the statistical significance. (**D**) Aβ1-42 oligomer induced changes in proinflammatory cytokines in BV2 cell line. $n=3$. TNF-α: $^{*}p=0.0329$, $^{**}p=0.0039$, $^{***}p=0.0005$ vs. C. IL-1β: $^{****}p<0.0001$ vs. C. One-way ANOVA was used to analyze statistical significance. (**E**, **F**) Effects of DOR and MOR on TNF-α and IL-1β in Aβ1-42 exposed BV2 cells. $n=3$. TNF-α: (E): $^{****}p<0.0001$, $^{***}p=0.0006$ vs. C. $^{\Delta\Delta}p=0.0061$ vs. A. (F): $^{***}p=0.0001$ or 0.0004, $^{**}p=0.0012$ vs. C. IL-1β: (E): $^{****}p<0.0001$, $^{**}p=0.0013$ vs. C. $^{\Delta\Delta}p=0.0071$ vs. A. (F): $^{***}p=0.0004$, $^{**}p=0.0011$ or 0.0051 vs. C. One-way ANOVA was used to analyze the statistical significance

AD- mimicked BV2 cell line (Supplementary 4 C), as well as the pro-inflammatory cytokines release (Fig. 4F).

Since the results gained from the AD mimicked BV2 cells are in accordance with our findings in APP/PS1 mice, our data consistently raises the possibility that DOR regulated AD neuroinflammation through microglial modulation.

DOR and MOR differentially regulated microglia in APP/PS1 mice and AD mimicked BV2 cells

To further determine the cellular and molecular effects of DOR and MOR in AD affected microglia, we used flow cytometry to sort $CD11^{+}CD45^{int-high}$ cells from the mouse brain (Supplementary 1). We found the percentage of the immune cells including microglia ($CD11b^{+}CD45^{int}$) and macrophage ($CD11b^{+}CD45^{high}$) was largely increased in the APP/PS1 mouse brain as compared to the WT mouse brain ($^{***}p<0.001$, vs. WT, Fig. 5A and B). UFP-512 administration significantly decreased microglia and macrophage amounts in APP/PS1 mouse brains ($^{\Delta\Delta}p<0.01$, vs. AD, Fig. 5A and B), while DAMGO-treated APP/PS1 mice exhibited excessive infiltration of microglia and macrophage which is similar to APP/PS1 mice treated with saline (Fig. 5A and B).

Then, we measured the expression of Iba1, a specific microglial marker which remarkably upregulates when microglia activate [26, 27]. By using immunofluorescent

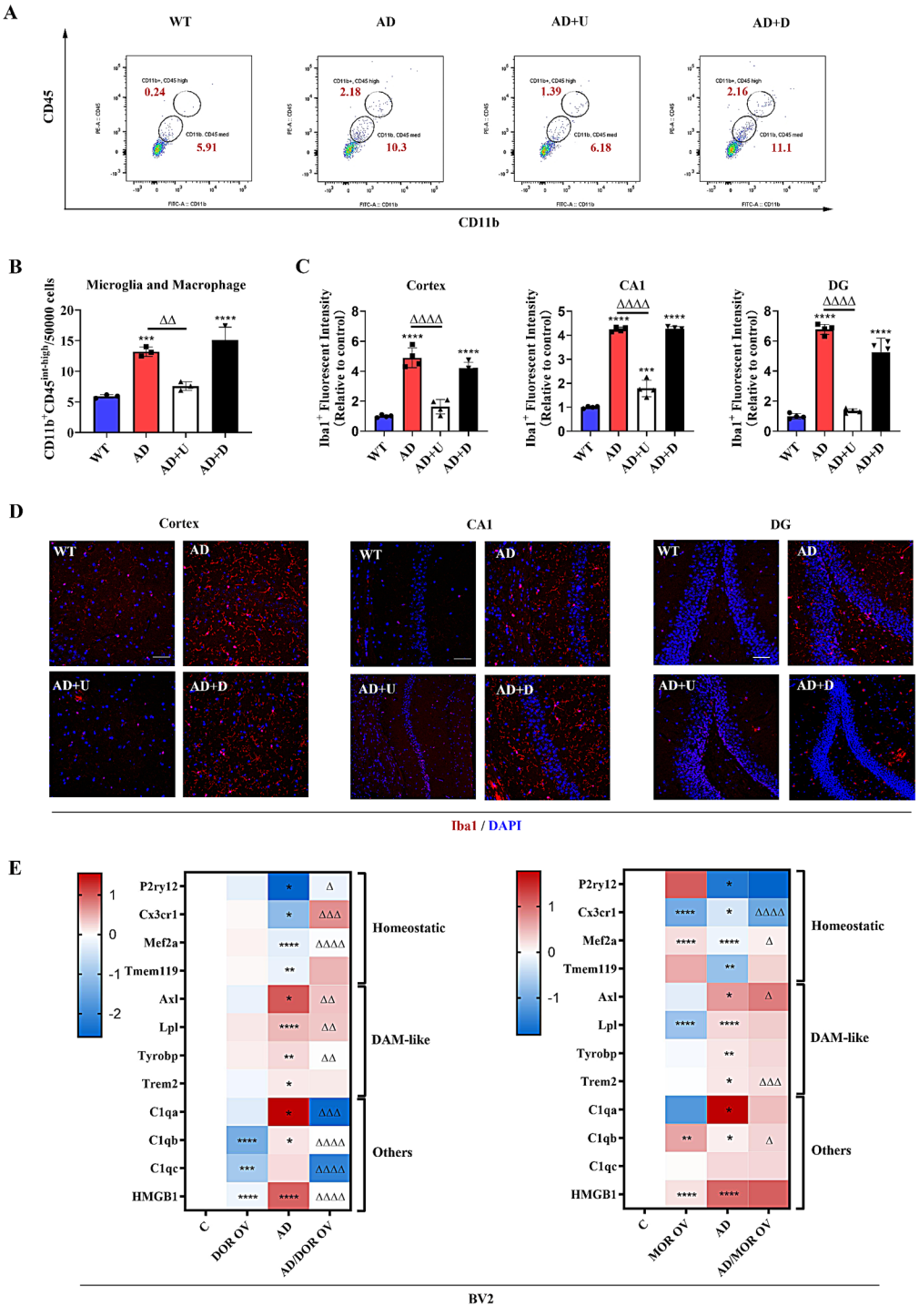

Fig. 5 DOR and MOR played different role in modulating microglia activation. (**A**,**B**) Effects of DOR and MOR on cerebral microglia/macrophages infiltration in APP/PS1 mice analyzed by flow cytometry. $n=3$. $^{***}p=0.0003$, $^{****}p<0.0001$ vs. WT. $^{\Delta\Delta}p=0.0018$ vs. AD. One-way ANOVA was used to analyze statistical significance. (**C**,**D**) Representative images of the Iba1 fluorescent staining and the quantification of Iba1$^+$ fluorescent intensity in the cortex and hippocampus of WT mice and APP/PS1 mice. $n=4$ mice per group for statistical analysis. Scale bar = 100 μm in panel. Cortex: $^{****}p<0.0001$ vs. WT. $^{\Delta\Delta\Delta\Delta}p<0.0001$ vs. AD. CA1: $^{****}p<0.0001$, $^{***}p=0.0003$ vs. WT. $^{\Delta\Delta\Delta\Delta}p<0.0001$ vs. AD. DG: $^{****}p<0.0001$ vs. WT. $^{\Delta\Delta\Delta\Delta}p<0.0001$ vs. AD. One-way ANOVA was used to analyze statistical significance. (**E**) Alternations in mRNA expression profile induced by DOR overexpression or MOR overexpression in normal BV2 cell line and Aβ1-42 exposed BV2 cell line. $n=3$. The p value was presented in Supplementary 8. Unpaired t test was used to analyze the statistical significance

staining, we found that Iba1 high-expressed cells were observed both in the cortex and hippocampus of APP/PS1 mice, but were not evident in WT mouse brain ($^{****}p < 0.0001$, vs. WT, Fig. 5C and D). UFP-512 largely reduced the Iba1 fluorescent intensity in the cortex and hippocampus of APP/PS1 mice ($^{\Delta\Delta\Delta\Delta}p < 0.0001$, vs. AD, Fig. 5C and D), while the application of MOR agonist DAMGO showed inappreciable effects on the Iba1 fluorescent intensity both in the hippocampus and cortex of APP/PS1. We also employed another marker, Galectin-3 to further validate the DOR/MOR mediated modulation of microglial activation and immune response. The expression of Galectin-3 is highly correlated with microglial activation in response to neurodegenerative injury, or neuroinflammatory injury [28–30]. In the present work, immunofluorescence techniques were utilized to observe a remarkable increase in the fluorescent intensity of Galectin-3 within Iba1-labeled microglia of APP/PS1 mouse brains in contrast to WT mice ($^{****}p < 0.0001$ vs. WT, Supplementary 5). Administration of UFP-512 greatly attenuated the Galectin-3 fluorescent signal in the associated microglia ($^{\Delta\Delta\Delta}p < 0.001$ vs. AD, Supplementary 5). However, no obvious change in Galectin-3 within microglia was detected in APP/PS1 mice treated with DAMGO. All these results indicate that DOR, but not MOR, owns the ability to modulate immune responses, and microglial activation in the presence of AD pathologies.

To fully map the effects of DOR and MOR on AD-associated microglia, we overexpressed DOR or MOR in BV2 cell line by using lentiviral infection techniques, and then exposed these infected BV2 cells to the Aβ1-42 oligomer to mimic AD injury. The transcriptome sequencing results showed that compared to the negative control BV2 cells exposed to normal conditions (C), the BV2 cells exposed to Aβ1-42 oligomer exhibited a significant decrease in majority of microglial homeostatic genes including Cx3cr1, Mef2a, TMEM119 and P2ry12 ($^{*}p < 0.05$, $^{**}p < 0.01$, $^{****}p < 0.0001$ vs. C, Fig. 5E), and a remarkable increases in disease-associated microglia (DAM)-like genes including Axl, Lpl, Tyrobp and TREM2 ($^{*}p < 0.05$, $^{**}p < 0.01$, $^{****}p < 0.0001$ vs. C, Fig. 5E), suggesting a gradually activation of BV2 cell line when exposed to Aβ1-42 oligomer. Overexpressing DOR largely upregulated microglial homeostatic genes including Mef2a, Cx3cr1 and P2ry12 in AD-mimicked BV2 cell line ($^{\Delta}p < 0.05$, $^{\Delta\Delta\Delta}p < 0.001$, $^{\Delta\Delta\Delta\Delta}p < 0.0001$ vs. AD, Fig. 5E), and inhibited the microglial DAM-like transformation labeled by Axl, LPl and Tyrobp ($^{\Delta\Delta}p < 0.01$ vs. AD, Fig. 5E). On the other hand, overexpressing MOR showed a complex response to microglia gene signatures with downregulated Cx3cr1 and upregulated Mef2a, Axl and Trem2 in the AD-mimicked conditions ($^{\Delta}p < 0.05$, $^{\Delta\Delta\Delta}p < 0.001$, $^{\Delta\Delta\Delta\Delta}p < 0.0001$ vs. AD, Fig. 5E).

The different performance of DOR and MOR in microglia modulation was also revealed by their linkage with C1q, the critical initiator of classical complement cascade, which is required for oligomer Aβ-induced synapse loss in vivo and produced mainly by myeloid cells such as microglia [31, 32]. C1q consists of three genes (C1q A, B, C) that encode proteins with a collagen-like region and a globular domain [31]. As the Fig. 5E depicted, Aβ1-42 oligomer significantly increased C1qa and C1qb genes but did not obviously affect C1qc ($^{*}p < 0.05$ vs. C, Fig. 5E). DOR overexpressed BV2 cells showed a remarkable decrease in all three C1q genes, and this effect was more evident in AD pathologies ($^{****}p < 0.0001$, $^{***}p < 0.001$ vs. C, $^{\Delta\Delta\Delta\Delta}p < 0.0001$ vs. AD, Fig. 5E). Overexpressing MOR tended to upregulate C1qb, but did not seriously affect C1qa and C1qc ($^{**}p < 0.01$ vs. C, $^{\Delta}p < 0.05$ vs. AD, Fig. 5E).

Another gene that was significantly affected by the overexpression of DOR/MOR in BV2 cell line is HMGB1. HMGB1 protein was thought to play a significant role in extracellular signaling associated with inflammation and trigger activation of immune cells [33, 34]. Activated microglia and macrophages also secrete HMGB1, forming a positive feedback loop that exaggerates microglial inflammatory transformation and cell death. As the transcriptome sequencing indicated, Aβ1-42 oligomer exposure largely increased HMGB1 in the BV2 cells ($^{****}p < 0.0001$ vs. C, Fig. 5E). DOR overexpression significantly downregulated HMGB1 mRNA in the BV2 cells in both normal condition and AD-mimicked injury ($^{****}p < 0.0001$ vs. C, $^{\Delta\Delta\Delta\Delta}p < 0.0001$ vs. AD, Fig. 5E). In contrast, MOR overexpression upregulated HMGB1 in normal condition, but did not affect HMGB1 seriously in AD-like condition ($^{****}p < 0.0001$ vs. C, Fig. 5E).

DOR participated in the regulation of HMGB1/NF-κB signaling pathway in AD mimicked BV2 cell line

Since DOR activation effectively inhibited AD-like pathology induced microglia activation and inflammatory response, we next focused on exploring its potential pharmacological mechanism. Based on the combined sequencing results gained from AD mimicked BV2 cell line with DOR or MOR overexpression (Fig. 5E), we firstly investigated the alternation in HMGB1 protein mediated by DOR or MOR in AD-affected microglia. In contrast to the significant increase in HMGB1 mRNA induced by Aβ1-42 oligomer as the sequencing results suggested, the amounts of HMGB1 protein in AD affected BV2 cells did not shown any significant change (Fig. 6A and C). Reduced HMGB1 expression occurred in the BV2 cell line treated with DOR agonist UFP-512 ($^{\Delta\Delta}p < 0.01$ vs. AD, Fig. 6A and C) and BV2 cell line overexpressing DOR ($^{*}p < 0.05$, vs. NC207, Fig. 6D and F) exposed to Aβ1-42 oligomer. Knocking down DOR or overexpressing MOR in AD mimicked BV2 cell line enhanced

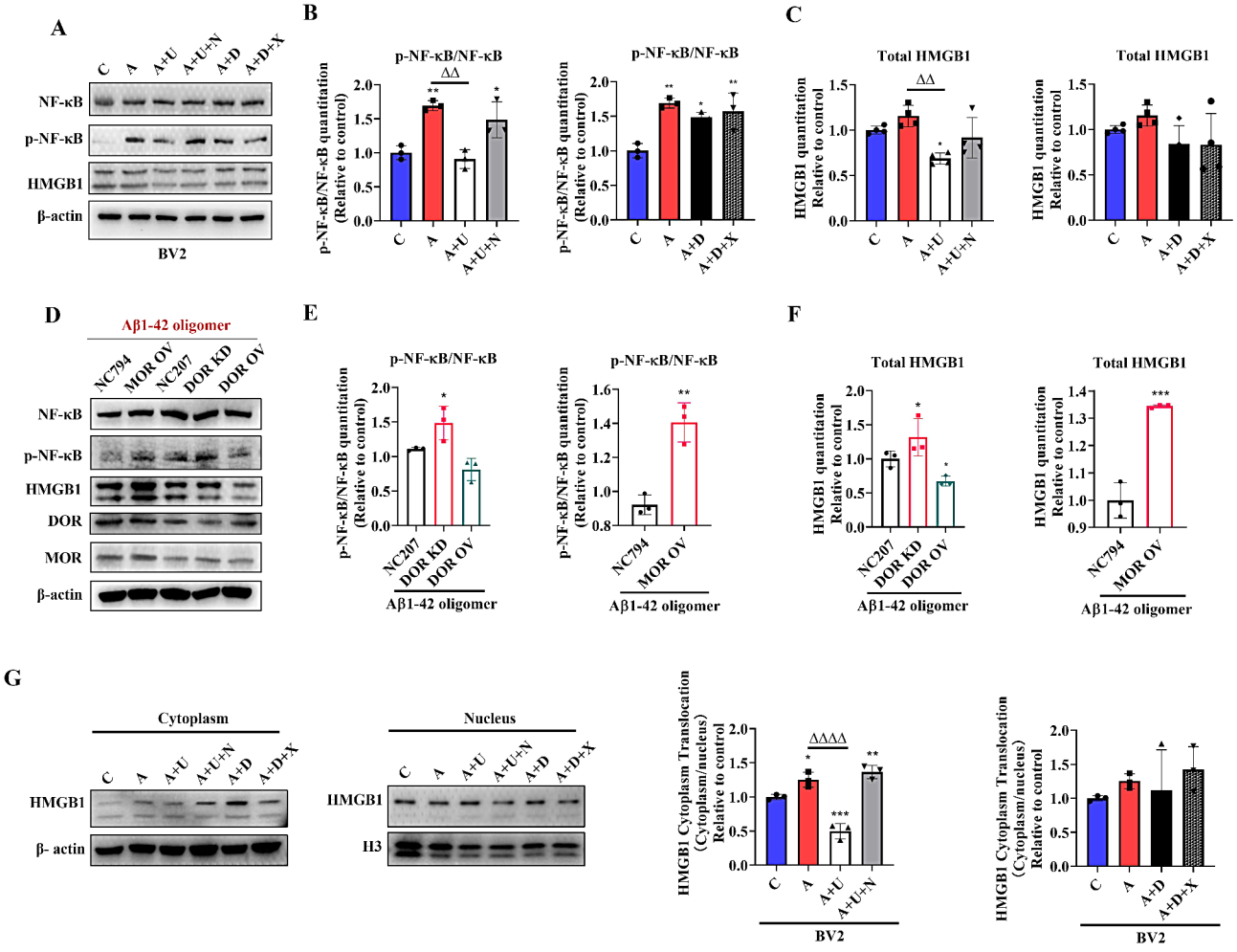

Fig. 6 DOR regulated HMGB1/NF-κB axis signaling pathway in AD mimicked BV2 cells. NC207: BV2 cells infected with lentivirus containing negative control 207 shRNA as the negative control for DOR; DOR KD: BV2 cells infected with lentivirus containing shRNA knocking down DOR; DOR OV: BV2 cells infected with lentivirus overexpressing DOR; NC794: BV2 cells infected with lentivirus containing negative control 794 shRNA as the negative control for MOR; MOR OV: BV2 cells infected with lentivirus overexpressing MOR. (**A-C**) Representative Western blot and quantification which show the effects of DOR and MOR activity alterations on HMGB1 and phosphorylation of NF-κB p65 protein level in BV2 cells. (B): $^{**}p = 0.0036$ or 0.0023 or 0.0075, $^{*}p = 0.0274$ or 0.0184 vs. C. $^{\Delta\Delta}p = 0.0016$ vs. A. $n = 3$. (C): $^{*}p = 0.0239$ vs. C. $^{\Delta\Delta}p = 0.0014$ vs. A. $n = 4$. One-way ANOVA was used to analyze the statistical significance both in 6B and 6 C. (**D-F**) Representative Western blot and quantification of the effects of DOR and MOR on HMGB1 and phosphorylation of NF-κB p65 protein level in BV2 cells. $n = 3$. (E): Left panel: $^{*}p = 0.0336$ vs. NC207. Right panel: $^{**}p = 0.0029$ vs. NC794. (**F**): Left panel: $^{*}p = 0.0136$ or 0.0145, vs. NC207. Right panel: $^{***}p = 0.0008$ vs. NC794. The unpaired t test was used to analyze the statistical significance both in 6E and 6 F. (**G**) Representative Western blot and quantification of HMGB1 cytoplasmic translocation in BV2 cells. $n = 3$. $^{*}p = 0.0454$, $^{**}p = 0.0063$, $^{***}p = 0.0008$ vs. C. $^{\Delta\Delta\Delta\Delta}p < 0.0001$, vs. A. One-way ANOVA was used to analyze statistical significance

HMGB1 expression ($^{*}p < 0.05$ vs. NC207, $^{***}p < 0.001$ vs. NC794, Fig. 6D and F), while treating BV2 cells with UFP-512 plus naltrindole, DAMGO or DAMGO plus naltrexone had no significant effects on HMGB1 expression. Moreover, we measured crucial proteins in HMGB1 related neuroinflammatory signaling pathway: NF-κB, using Western blot (Fig. 6A, B, D and E). The results showed the ratio of phosphorylated NF-κB/ NF-κB significantly increased in Aβ1-42 oligomer exposed BV2 cell line ($^{**}p < 0.01$, vs. C, Fig. 6A and B). DOR activation, but not MOR activation reversed this change ($^{\Delta\Delta}p < 0.01$, vs. A, Fig. 6A and B). Genetically knocking-down DOR or overexpressing MOR in AD mimicked BV2 cells also enhanced NF-κB p65 phosphorylation ($^{*}p < 0.05$, vs. NC207, $^{**}p < 0.01$ vs. NC794, Fig. 6D and E). It has been reported that HMGB1 is mainly located in the nuclei of cells, and its secretion and translocation from nucleus to cytoplasm are involved in the neuroinflammation-related signaling pathway [33]. Although Aβ1-42 oligomer-mediated HMGB1 alternations did not reach a significance level, AD mimicked BV2 cell line showed an enhanced translocation of HMGB1 from nucleus to cytoplasm ($^{*}p < 0.05$, vs. C, Fig. 6G). DOR activation largely inhibited HMGB1 release in the cytoplasm ($^{\Delta\Delta\Delta\Delta}p < 0.0001$, vs. A,

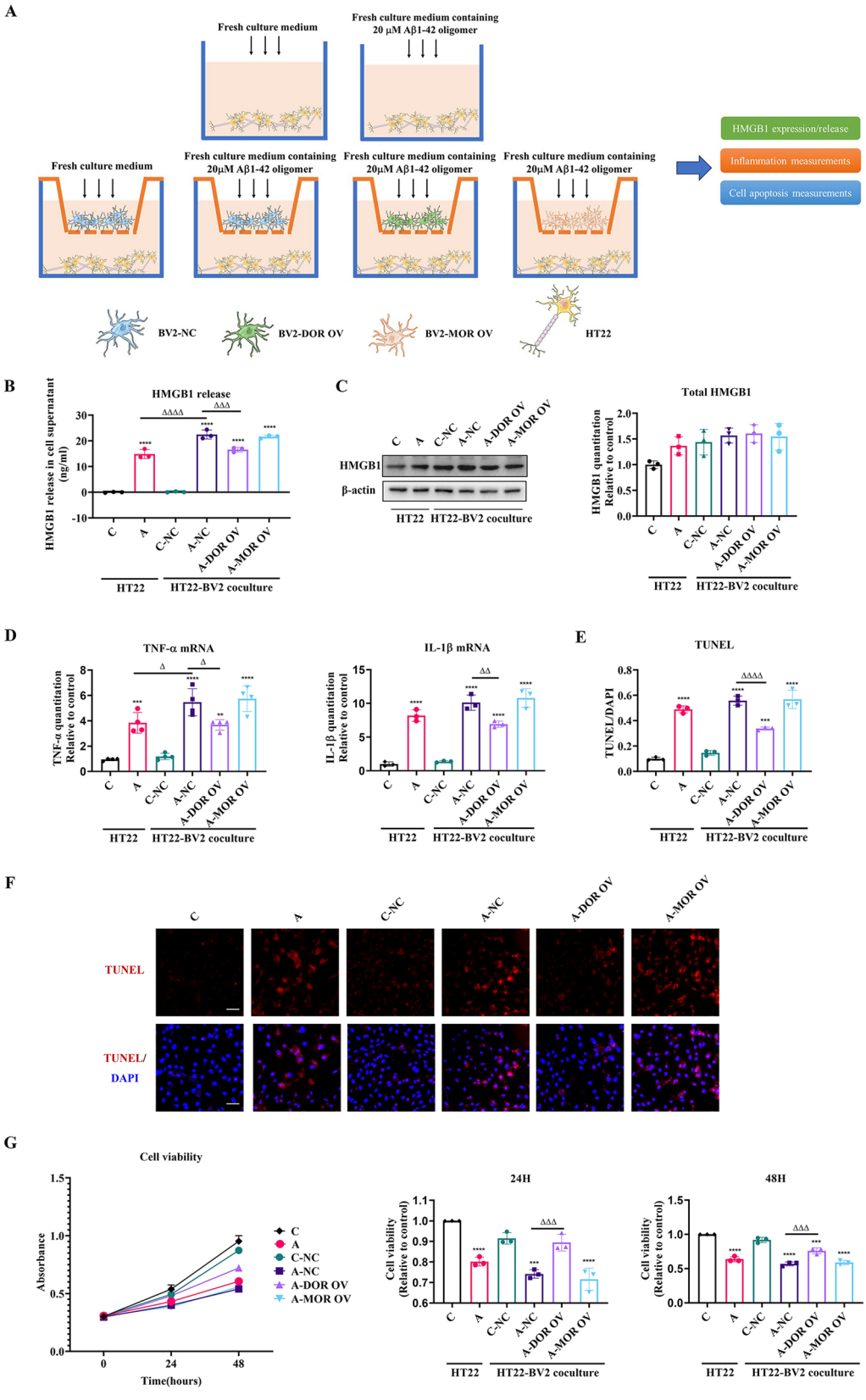

Fig. 7 (See legend on next page.)

(See figure on previous page.)

Fig. 7 DOR protected neurons in HT22-BV2 co-culture system via modulating microglia. C: the control HT22 cells cultured without BV2 cells; A: the HT22 cells cultured under Aβ1-42 oligomer injury without BV2 cells; C-NC: the control HT22 cells co-cultured with BV2 cells infected with negative control lentivirus; A-NC: the HT22 cells co-cultured with BV2 cells infected with negative control lentivirus under Aβ1-42 oligomer exposure; A-DOR OV: the HT22 cells co-cultured with BV2 cells infected with lentivirus overexpressing DOR exposed to Aβ1-42 oligomer; A-MOR OV: the HT22 cells co-cultured with BV2 cells infected with lentivirus overexpressing MOR exposed to Aβ1-42 oligomer. (**A**) Schematic diagram showing HT22-BV2 co-culture system and the grouping. (**B**) Overexpressing DOR or MOR in BV2 cells induced the alternations in HMGB1 release in culture medium in HT22-BV2 coculture system. $n = 3$. $^{****}p < 0.0001$ vs. C; $^{****}p < 0.0001$ vs. C-NC; $^{\Delta\Delta\Delta\Delta}p < 0.0001$ vs. A; $^{\Delta\Delta\Delta}p = 0.0003$ vs. A-NC. One-way ANOVA was used to analyze statistical significance. (**C**) Effects of DOR-overexpressed BV2 cells and MOR-overexpressed BV2 cells on HMGB1 expression in HT22. $n = 3$. One-way ANOVA was used to analyze statistical significance. (**D**) Effects of overexpressing DOR or MOR in BV2 cells on inflammatory status of HT22 in microglia-neuron co-culture system. $n = 3$. TNF-α: $^{***}p = 0.0003$ vs. C; $^{****}p < 0.0001$, $^{**}p = 0.0013$ vs. C-NC; $^{\Delta}p = 0.0466$ vs. A; $^{\Delta}p = 0.0242$ vs. A-NC. IL-1β: $^{****}p < 0.0001$ vs. C; $^{****}p < 0.0001$ vs. C-NC; $^{\Delta\Delta}p = 0.006$ vs. A-NC. One-way ANOVA was used to analyze statistical significance. (**E**,**F**) TUNEL staining and statistics of TUNEL-positive cells in HT22-BV2 co-culture system. $n = 3$. Scale bar = 100 μm in panel. $^{****}p < 0.0001$ vs. C; $^{****}p < 0.0001$, $^{***}p = 0.0003$ vs. C-NC; $^{\Delta\Delta\Delta\Delta}p < 0.0001$ vs. A-NC. One-way ANOVA was used to analyze statistical significance. (**G**) Representative time course and bar graph of cell viability alternations in each group. $n = 3$. 24 H: $^{****}p < 0.0001$ vs. C; $^{****}p < 0.0001$, $^{***}p = 0.0003$ vs. C-NC; $^{\Delta\Delta\Delta}p = 0.0009$ vs. A-NC. 48 H: $^{****}p < 0.0001$ vs. C; $^{****}p < 0.0001$, $^{***}p = 0.0009$ vs. C-NC; $^{\Delta\Delta\Delta}p = 0.0002$ vs. A-NC. One-way ANOVA was used to analyze statistical significance

Fig. 6G), and the addition of DOR antagonist naltrindole reversed this change. MOR activity did not appreciably affect HMGB1 translocation in AD-affected BV2 cells.

DOR activation mitigated HMGB1-mediated microglial inflammatory response and protected neurons against injuries in AD mimicked neuron-microglia co-culture system

The next question we asked is whether DOR-mediated neuroprotection is, at least partly, dependent on DOR's regulation of microglia and microglial HMGB1/NF-kB signaling pathway. We thus established a model of microglia/ neuron co-culture and set neuronal cells with no co-cultured BV2 as a control (Fig. 7A), to investigate the microglia-mediated effects on neurons. Firstly, we collected the supernatant in this coculture system and measured the HMGB1 release by using ELISA kit. As Fig. 7B showed, Aβ1-42 oligomer induced a significant increase in extracellular HMGB1 release ($^{****}p < 0.0001$, vs. C or C-NC, Fig. 7B), and the release became more evident in the HT22-BV2 coculture system ($^{\Delta\Delta\Delta\Delta}p < 0.0001$, vs. A, Fig. 7B). Overexpressing DOR in BV2 cells sharply reduced the HMGB1 release to the supernatant of the coculture system ($^{\Delta\Delta\Delta}p < 0.001$, vs. A-NC, Fig. 7B), suggesting that DOR is efficient in regulating HMGB1 extracellular release by modulating microglia in AD conditions. Meanwhile, we found although the amount of HMGB1 in HT22 cells tended to increase when exposed to Aβ1-42 oligomer injury, the crosstalk of DOR overexpressed-BV2 or MOR overexpressed-BV2 with HT22 did not significantly alter HMGB1 expression in HT22 cells (Fig. 7C).

Since HMGB1 was regarded as an important inflammatory mediator by binding with neuronal receptors and inducing neuroinflammation [35], we further examine the inflammatory status and cell injuries in HT22 cells in each group. As Fig. 7D depicted, Aβ1-42 oligomer largely increased the pro-inflammatory cytokines TNF-α and IL-1β mRNA levels in HT22 cells, especially in HT22-BV2 coculture model ($^{***}p < 0.001$, $^{****}p < 0.0001$, vs. C; $^{****}p < 0.0001$ vs. C-NC; $^{\Delta}p < 0.05$, Fig. 7D). Overexpressing DOR in microglia effectively inhibited TNF-α and IL-1β level in Aβ1-42 oligomer exposed HT22 ($^{\Delta}p < 0.05$, $^{\Delta\Delta}p < 0.01$, vs. A-NC, Fig. 7D), while overexpressing MOR in microglia did not appreciably affect the Aβ1-42 oligomer induced neuroinflammatory status (Fig. 7D). In accordance with the alternations in neuroinflammation, the TUNEL-positive HT22 cells remarkably increased in the Aβ1-42 oligomer treated group ($^{****}p < 0.0001$, vs. C or C-NC, Fig. 7E), DOR-overexpressed microglia largely attenuated TUNEL-positive HT22 cells in this co-culture system ($^{\Delta\Delta\Delta\Delta}p < 0.0001$, vs. A-NC, Fig. 7E and F). In contrast, overexpressing MOR did not significantly alter the amount of TUNEL-staining in the HT22 cells (Fig. 7E and F). In addition, both AD affected HT22 or HT22-BV2 co-culture AD model exhibited a decreased cell viability compared to the control ($^{****}p < 0.0001$ vs. C, $^{****}p < 0.0001$, $^{***}p < 0.001$ vs. C-NC, Fig. 7G). The crosstalk between HT22 and DOR-overexpressed BV2 effectively upregulated the cell viability of co-culture system both in 24 h and 48 h timepoint ($^{\Delta\Delta\Delta}p < 0.001$ vs. A-NC, Fig. 7G), while MOR-overexpressed microglia did not appreciably affect HT22 cell viability both at 24 h and 48 h timepoints (Fig. 7G).

Taken together, our data suggest that DOR's inhibition on neuroinflammation and DOR-mediated neuroprotection are substantially reliant on DOR's impact on microglia and specific modulation of HMGB1.

DOR activation inhibited HMGB1 release in APP/PS1 mouse brain by downregulating HMGB1 in the microglia

Our in vivo study further supports this conclusion. The seq-RNA analysis showed that the HMGB1 mRNA level was upregulated in the brain of APP/PS1 mice, especially in the hippocampal region ($^{***}p < 0.001$, vs. WT, Supplementary 6 A). Consistently, DOR agonist UFP-512 administration effectively reduced HMGB1 mRNA level both in the cortex and hippocampus of APP/PS1 mice, while MOR agonist DAMGO did not ($^{\Delta}p < 0.05$, $^{\Delta\Delta\Delta\Delta}p < 0.0001$ vs. AD, Supplementary 6 A). To clarify if

DOR-mediated regulation of HMGB1 is majorly acting on microglia or neurons, we conducted Iba1/ NeuN/ HMGB1 immunofluorescent staining to investigate the effects of DOR and MOR on HMGB1 in both neurons and microglia of the mouse brain. As Fig. 8 showed, both neurons (labeled with NeuN) and microglia (labeled with Iba1) expressed certain amounts of HMGB1. Since the proportion of HMGB1 in microglia was higher than it in neurons in APP/PS1 mouse brains ($^{*}p < 0.05$, vs. neurons in AD, Fig. 8A and B), the microglia are likely the major cell type expressing HMGB1 in the AD brain. Consistent with our in vitro study, the administration of UFP-512 induced a significant decrease in HMGB1 in microglia in AD mouse brain ($^{\Delta}p < 0.05$ vs. microglia in AD, Fig. 8B), and the HMGB1 protein in neurons also reduced by UFP-512, though it did not reach a significant level. It is worth noting that extracellular HMGB1 release was observed in all groups, which was especially evident in AD mice and AD mice injected with DAMGO. To further validate DOR/MOR mediated alternations of HMGB1 in AD mice, we conducted HMGB1 immunohistochemical staining. As depicted in Supplementary 6B-6D, a slight increase in HMGB1-positive cells were detected in the APP/PS1 mice, which is evident in the CA1 region. The application of UFP-512 largely inhibited HMGB1 expression both in the cortex and hippocampus of APP/PS1 mice ($^{\Delta}p < 0.05$, vs. AD, Supplementary 6B), while MOR agonist DAMGO did the opposite, i.e., leading to a significant increase in HMGB1 protein secretion ($^{**}p < 0.01$, vs. WT, Supplementary 6B). Notably, AD also induced HMGB1 translocation from nucleus to cytoplasm or extracellular ($^{****}p < 0.0001$, vs. WT, Supplementary 6 C) in the mouse CA1, DG and cortex regions, which could be reversed by UFP-512 treatment ($^{\Delta\Delta\Delta}p < 0.001$, vs. AD, Supplementary 6 C), but not by DAMGO treatment.

In APP/PS1 mouse cortex and hippocampus, the NF-κB p65 DNA binding activities were also evaluated using NF-κB p65 transcription factor assay. As Fig. 8C showed, NF-κB p65 DNA binding activity up-regulated in APP/PS1 mouse brain ($^{****}p < 0.0001$, vs. WT, Fig. 8C) and largely decreased in APP/PS1 mice treated with DOR agonist UFP-512 ($^{\Delta\Delta\Delta}p < 0.001$, $^{\Delta\Delta\Delta\Delta}p < 0.0001$, vs. AD, Fig. 8C).

Combined with these in vivo data in APP/PS1 mice, we identify DOR as a target for neuroprotection in AD by attenuating microglial inflammatory responses and inhibiting HMGB1 signaling pathway.

Discussion

Our previous work has revealed the different roles of DOR and MOR in BACE1 regulation in Aβ1-42 oligomer mimicked AD cell model [15]. Following this clue, we used the 9-month-old APP/PS1 mice in this work to further evaluate the effects of DOR and MOR on AD brains. APP/PS1 mice exhibited declined cognitive ability and increased Aβ accumulation in the brain, which could be ameliorated by DOR activation using UFP-512, while MOR activation showed a short-time effect or no effect. RNA-seq analysis further revealed that DOR activation effectively corrected AD induced genetic changes and inhibited cell apoptosis in APP/PS1 mice. Compared to MOR, DOR activation also inhibited microglial activation and microglial inflammatory response in AD pathologies, which was consistently confirmed by in vivo and in vitro work. Moreover, we found that DOR's negative regulations of HMGB1/NF-κB signaling pathway may mitigate the neuroinflammation and rescue neurons from AD injury. Our novel findings strongly suggest a beneficial effect of DOR signaling on AD.

DOR, MOR and KOR are three classical members of opioid receptors. Early genetic studies on DNA methylation have revealed that the genes encoding DOR, MOR and KOR showed higher levels of methylation and dysregulated in AD patients, which suggests their potential involvement in AD pathogenesis [36, 37]. There is fewer clue cueing the direct effects of KOR on AD pathologies. However, it is very interesting to explore the cellular and molecular underpinnings linking DOR/MOR with AD because of the evidence directly connecting DOR/MOR with Aβ production and the clues for their complex roles in AD pathologies [15, 36, 38, 39]. Teng et al. [40] claimed that DOR activation promoted the processing of Aβ precursor protein (APP) by forming complex with β-site APP-cleaving enzyme 1 (BACE1) and gamma-secretase, thus contributing to the AD pathologies and AD-related cognitive impairment. Compared to DOR, MOR activation was thought to attenuated Aβ induced neurotoxicity through mTOR signaling [39]. In contrast to their work, our group and Wang's group reported a very different role of DOR and MOR in Aβ regulation by using more specific DOR agonist [15, 41]. We found long-term exposure of the cells with DOR agonists, but not MOR agonists (> 24 h), largely reduced BACE1 expression and Aβ42 production, instead of promoting it. To further clarify the role of DOR and MOR in AD, the present results from APP/PS1 mice show the first evidence that DOR and MOR populations were differentially altered in the hippocampus and cortex respectively, with a major decrease of MOR in the cortex and a slight decrease of DOR in the hippocampus. Since the hippocampus is the main site responsible for learning and memory, while the cortex performs complex functions in behavioral, emotional, sensory, and cognitive regulation, both of them are vulnerable to AD pathologic attack [42, 43] and the alternations of DOR and MOR in these regions may affect the development of the symptomatology of AD. Consistent with our work in APP/PS1 mice, autoradiographic studies of postmortem brains of AD patients have shown a

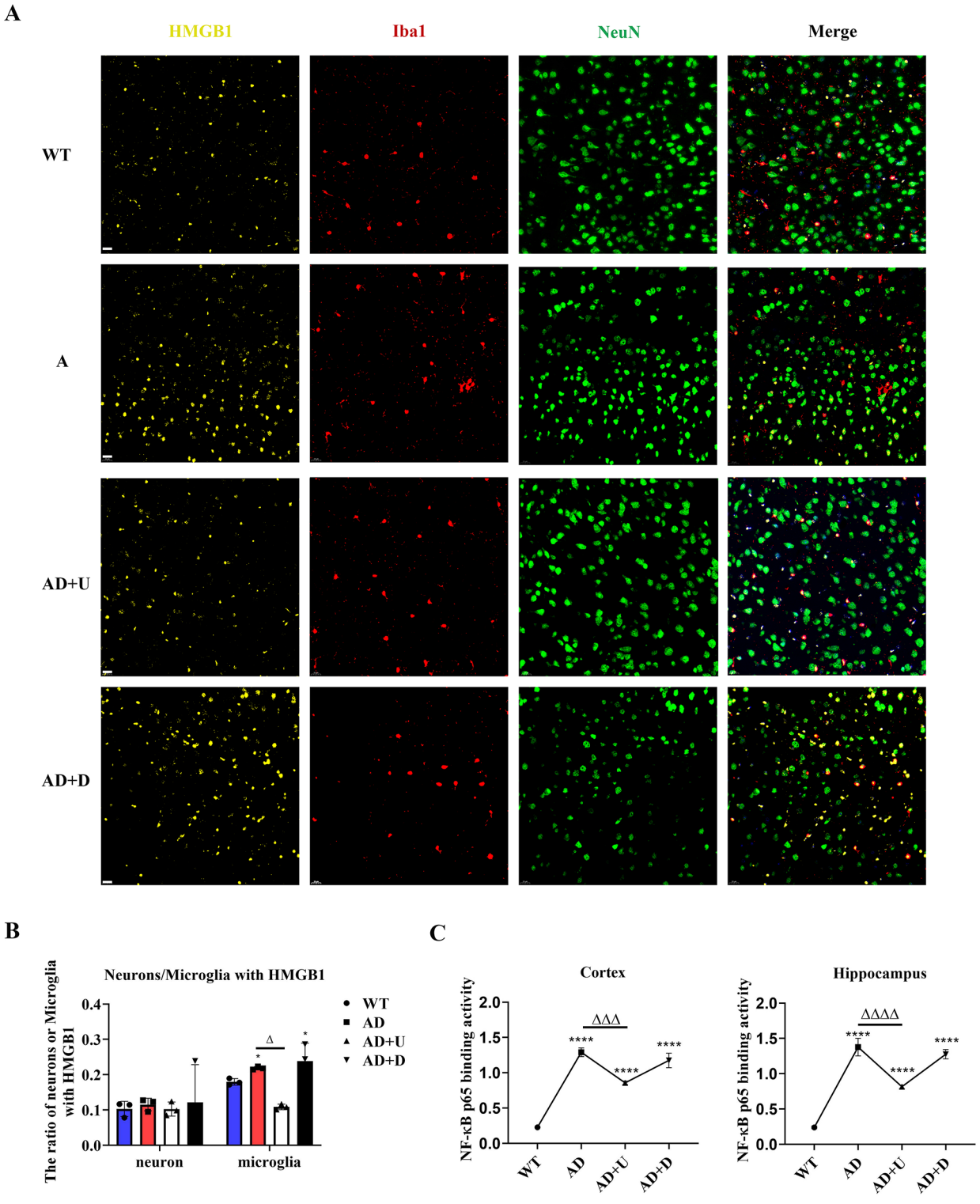

Fig. 8 DOR activation remarkably decreased HMGB1 in microglia versus neurons in APP/PS1 mouse brain. (**A**, **B**) Immunofluorescence staining and statistics of HMGB1 ration in neurons versus microglia. $n = 3$ mice per group for statistical analysis. Scarle bar = 20 μm. $^{*}p = 0.0419$ vs. neurons in AD; $^{*}p = 0.0192$ vs. neuron in AD + D; $^{\Delta}p = 0.0426$ vs. microglia in AD. Two-way ANOVA was used to analyze the statistical significance. (**C**) NF-κB p65 binding activities in each mouse group. $n = 3$. Cortex: $^{****}p < 0.0001$ vs. WT. $^{\Delta\Delta\Delta}p = 0.0001$ vs. AD. Hippocampus: $^{****}p < 0.0001$ vs. WT. $^{\Delta\Delta\Delta\Delta}p < 0.0001$ vs. AD. One-way ANOVA was used to analyze statistical significance

decreased density of DOR and MOR, especially in the hippocampus and cortex of AD patients as compared to those of the control populations [9]. These findings on expressional changes in the endogenous opioid system, from living APP/PS1 mice to postmortem of AD patients, imply a potential impact of opioid-based interventions on AD.

MWM and novel object recognition tests are two major approaches to evaluate the cognitive ability of aging mice. Specific activation of DOR effectively improved cognitive performance of APP/PS1 mice but that of MOR did not. This is the first time to show that a potent, and specific DOR agonist has a positive impact on AD, which is interesting and provoking. Past studies implied a destructive role of DOR in AD progression based on the evidence that DOR antagonist naltrindole ameliorated Aβ-dependent behavioral deficits in 4–6 old APP/PS1 mice [40, 44, 45]. However, growing evidence indicates that behavioral and cognitive deficient became evident in APP/PS1 mice at least in 8 months [46, 47]. Our work used 9-month-old APP/PS1 mice and convincingly demonstrated a therapeutic effect of DOR activation on the APP/PS1 mice. Apparently, DOR activation, but not inhibition, brings a stronger and prolonged benefit on the late stage of AD progress.

Consistent with our previous findings in AD cell model [15], insoluble Aβ42 in the hippocampus of APP/PS1 mice was significantly attenuated by DOR activation. Aβ plaques and cortical insoluble Aβ42 were also reduced in certain extent by the administration of DOR agonist. Although MOR activation also showed an inhibitory effect on soluble Aβ42 in the hippocampal region of APP/PS1 mice, more aggregated Aβ42 and Aβ plaques were found in the same brain region, suggesting the core role of insoluble Aβ in the formation of amyloid plaques. Moreover, our RNA-seq analysis and TUNEL staining further demonstrated that compared to MOR, DOR exhibited stronger protective capacity against AD.

Microglia-mediated neuroinflammation is one of the critical factor for AD pathology as shown in our previous studies [17] and those of others [48–51]. Immune triggering is a major function of microglia. Microglia constantly surveys surrounding milieu for injury signals such as tauopathy or amyloid deposition, initiating immune responses including releasing inflammatory cytokines, increasing immune cells infiltration and hyperactivating these cells [50, 52]. Since microglia is the major immune cell type in the CNS [53] and DOR activation effectively ameliorated the neuroinflammation in APP/PS1 mice as shown in the preset work, we further elucidate the effects of DOR on microglia. Notably, compared to the unappreciable performance of MOR in macrophage infiltration, microglia activation and pro-inflammatory cytokines release, DOR exhibited a unique power in modulating microglial activation and microglia-related immune responses under AD exposure. More precise work to explore the relationship between DOR/MOR and microglia were conducted in BV2 cell line. The work of scRNA-seq revealed an increased proportion of homeostasis gene subgroup and decreased proportion of DAM-like gene subgroup in DOR overexpressed BV2 cell line, providing more evidence to support DOR's inhibitory regulation of microglial activation. In contrast, the RNA-seq results of MOR overexpressed BV2 versus the control BV2 highlight the complexity of MOR action in microglia and AD affected microglia, which needs more work to clarify its real effects.

Except for the different expression profile of DOR versus MOR in microglial homeostasis gene subgroup and DAM-like gene subgroup, DOR and MOR also differentially regulated C1qa, C1qb, C1qc and HMGB1. C1qa, C1qb and C1qc constitute the C1q. Indeed, emerging evidence indicates that upregulated C1q were observed in the brain of multiple AD animal model [32, 50, 54]. The increased C1q was associated with aberrant activation of complement cascade, synapses loss and memory defects [32, 54, 55]. In the present work, KEGG pathway analysis shows that the AD mice treated with UFP-512, but not DAMGO, had a significant enrichment of DEGs related to complement and coagulation cascades. Combined with the in-vivo data, the seq-results from BV2 cells further suggest that DOR overexpression was correlated with the decrease in the mRNA levels of C1qa, C1qb, and C1qc. The in vivo and in vitro studies consistently raise the possibility that DOR, but not MOR, has a potential tight linkage with C1q in microglia in AD pathologies, which needs to be further explored.

The results of RNA-seq analysis of BV2 cells also imply a contrasting relationship between HMGB1 and DOR versus HMGB1 and MOR in AD. It has been reported that HMGB1 is elevated in the cerebrospinal fluid (CSF) of human with mild cognitive impairment (MCI) [56–58]. Both Aβ1-42 oligomer and pathological tau oligomers can trigger immune cells such as microglia and macrophage actively secrete HMGB1 [59, 60]. In several animal models of inflammation, HMGB1 triggers inflammatory pathways as follows: inflammation promotes more HMGB1 translocating from nuclear to cytoplasm or extracellular in cerebral cells, together with the damaged or dead cells allow the release of HMGB1 extracellularly. The increased extracellular HMGB1, as a damage-associated molecular pattern (DAMP), binds to receptors such as receptor for advanced glycation end products (RAGE) or toll like receptor (TLR). These activated receptors then trigger the activation of NF-κB pathway and initiate the inflammatory responses, forming a HMGB1-NF-κB mediated vicious circle [59–61]. Our present work has well demonstrated that DOR activation or overexpression

could evidently inhibit HMGB1 production, translocation and extracellular release, which effectively prevents the signaling transduction through HMGB1/NF-κB axis in BV2 cells. DOR's regulations of HMGB1 were also observed in a microglia-neuron coculture system, which induce an overall neuroprotective response to neurons through a major modulation of microglia. Intriguingly, in this coculture system, the amount of HMGB1 in the hippocampus neurons HT22 was not seriously affected by DOR overexpression or MOR overexpression in BV2, but the HT22 cells were still protected from apoptosis and exhibited decreased inflammatory status. One explanation is that DOR overexpression in BV2 cells attenuates the extracellular release of HMGB1 under AD injury, and thus reduced the binding of the free HMGB1 with its receptors in HT22 cells to activate NF-κB pathway. Consequently, the neuroinflammation was inhibited and the HT22 cells were saved by DOR intervened microglia-neuron crosstalk on AD pathology.

In this work, we also observed more significant alternations in HMGB1 release in microglia versus neurons in UFP-512 treated APP/PS1 mice, which validates our hypothesis that DOR-mediated neuroprotection is partly dependent on DOR's modulation of microglia and regulation of HMGB1. More recently, a new drug called PLX5622 (the inhibitor of CSF1R) has been proved to effectively eliminate microglia in mice without evident side effects [62]. We will further clarify whether DOR-mediated neuroprotection against AD injury is dependent on its modulations of microglia with this new model in our future work.

Limitation of the study

Our study has limitations. Indeed, we validate that DOR-mediated neuroprotection is critically dependent on DOR's regulation of microglial function and HMGB1 signaling. This is documented by evidence that a significant alternation in HMGB1 occurred in microglia rather than neurons in the AD mice treated with UFP-512. This observation is further supported by the finding that DOR overexpressing in BV2 cells severely affected HMGB1 release and neuroinflammatory status in a microglia-neuron coculture system. However, it is difficult to state DOR's regulation of microglia and HMGB1 is the sole mechanism behind DOR-mediated protection against AD injury. As shown in our previous work, DOR activation could reduce BACE1 expression and activity by directly targeting neuron, contributing to decreased Aβ production [15]. Therefore, it is likely that DOR agonism improves AD outcomes by targeting both neurons and microglia. One strategy to elucidate this point is to simultaneously examine HMGB1 and BACE1 in AD neurons and microglia at cellular and molecular level and comparatively test the effects of DOR activation on their changes and the degree of the improvement of AD injury in both in vivo and in vitro models. We have proposed the work for this research goal.

Moreover, since we have well demonstrated that UFP-512 treatment effectively reduced the microglial DAM-like phenotype, and inhibited microglial activation in AD mouse model, it is interesting to further explore whether the reduction in DAM-like subgroup microglia and activated microglia are associated with attenuated phagocytic activities of microglia and worsen amyloid pathologies. Indeed, we have unlocked this puzzle in our new work, and found a tight linkage between DOR, C1q and microglia phagocytosis in that work, which further supports the beneficial role of DOR agonism in AD rather than its destructive role. Given that is a whole complex story, we will present our novel findings in our next publication.

Conclusion

In summary, our novel findings uncover previously unknown roles of DOR and MOR in AD pathologies at behavioral, molecular, and cellular levels. We discover that DOR targets HMGB1 in microglia, thus attenuating inflammation and rescuing neurons from apoptosis and loss. Since DOR is a critical stabilizer of microglia in neuroinflammatory events, a deep investigation into the crosstalk among DOR, microglia function, and AD pathologies may potentially shed a new light on AD therapy.

Abbreviations

AD	Alzheimer's disease
DOR	δ-opioid receptor
MOR	μ-opioid receptor
Aβ	β-amyloid
HMGB1	High mobility group protein B1
ACH	Acetyl choline
KOR	κ-opioid receptor
APP/PS1	Aβ precursor protein/presenilin-1
TUNEL	Terminal deoxynucleotidyl transferase dUTP nick-end labeling
NICR	National Infrastructure of Cell Line Resource
PVDF	Polyvinylidenedifluorid
CTFB	Complete Transcription Factor Binding Assay Buffer
PCR	Polymerase chain reaction
FDR	False discovery rate
ANOVA	Analysis for variance
BACE1	β-site APP cleaving enzyme 1
DEGs	Differentially expressed gens
iNOS	Inducible nitric oxide synthase
CSF	Cerebrospinal fluid
RAGE	Receptor for advanced glycation endproducts
TLR	Toll like receptors
APP	Aβ precursor protein
BACE1	β-site APP cleaving enzyme 1
DAMP	Damage-associated molecular pattern
HFIP	Hexafluoroisopropanol

Supplementary Information

The online version contains supplementary material available at https://doi.org/10.1186/s13195-025-01682-1.

Supplementary Material 1: A Flow Cytometry gating strategy for the analysis of microglia and macrophages in the mouse brain. **(A)** The dot plot FSC-A versus FSC-H discriminates the doublet. **(B)** The morphological gating strategy refers to dot plot FSC-A versus SSC-A. **(C)** The dot plot CD45 versus CD11b identifies microglial subgroup and macrophage subgroup.

Supplementary Material 2: Immunofluorescent investigations of the distributions of DOR and MOR in WT mice brain versus APP/PS1 mice brain. Scale bar = 500 μm. **(B)** The quantification of the fluorescent intensity of DOR and MOR signaling in the cortical and hippocampal regions of WT versus AD mice brains. $n = 3$ mice per group for quantification. MOR: $^{**}p = 0.0046$ vs. WT; DOR: $^{***}p = 0.0003$ vs. WT. Unpaired t-test was used to analyze the statistical significance. **(C)** A probe trial was performed on Day 1. The number of mice crossing the target quadrant, and the time mice spent in the target quadrant were recorded. $n = 10$. Left panel: $^{***}p = 0.0008$, $^{**}p = 0.0019$ or 0.0037 vs. WT; Right panel: $^{*}p = 0.0392$ vs. WT. One-way ANOVA was used to analyze statistical significance.

Supplementary Material 3: KEGG analysis of DEGs of AD mice treated with DOR agonist UFP-512 compared to AD mice treated with saline in cortical and hippocampal regions.

Supplementary Material 4: Representative images illustrate the co-localization of Galectin 3 and Iba 1 staining in the brains of WT mice and APP/PS1 mice. $n = 3$ mice per group for statistical analysis. Scale bar = 20 μm in panel. $^{****}p$<0.0001 vs. WT. $^{\Delta\Delta\Delta}p = 0.0002$ vs. AD. One-way ANOVA was used to analyze statistical significance

Supplementary Material 5: Representative images illustrate the co-localization of Galectin 3 and Iba 1 staining in the brains of WT mice and APP/PS1 mice. $n = 3$ mice per group for statistical analysis. Scale bar = 20 μm in panel. $^{****}p$<0.0001 vs. WT. $^{\Delta\Delta\Delta}p = 0.0002$ vs. AD. One-way ANOVA was used to analyze statistical significance

Supplementary Material 6: DOR activation reduced HMGB1 expression and translocation in AD mouse model. **(A)** mRNA analysis of HMGB1 in the cortex and hippocampus of each mice group. $n = 3$. Cortex: $^{\Delta}p = 0.0251$ vs. AD. Hippocampus: $^{***}p = 0.0001$, $^{*}p = 0.0175$ vs. WT. $^{\Delta\Delta\Delta\Delta}p < 0.0001$ vs. AD. Two-way ANOVA was used to analyze the statistical significance. **(B-D)** Immunohistochemical staining and statistics of HMGB1 expression and translocation ratio from the nucleus in each mice group in vivo. $n = 3$ mice per group for quantification. Scale bar = 100 μm in panel. (B): $^{**}p = 0.003$ vs. WT. $^{\Delta}p = 0.0172$ vs. AD. (C): $^{****}p < 0.0001$, $^{**}p = 0.0013$ vs. WT. $^{\Delta\Delta\Delta}p = 0.0008$ vs. AD. One-way ANOVA was used to analyze the statistical significance both in S5B and S5C.

Supplementary Material 7: Raw data for Western blot.

Supplementary Material 8: Figure 5E statistical analyses.

Acknowledgements
Not applicable.

Author contributions
Yuan Xu and Ying Xia conceived and designed the experiments; Yuan Xu, Jiahui Li and Naiyuan Shao performed the experiments and analysed the data; Yuan Xu, Yilin Yang, Ya Peng, Naiyuan Shao and Ying Xia contributed reagents/materials/analysis tools; Ying Xia, Feng Zhi, Ronghua Chen and Ya Peng supervised the conduct of the work; Yuan Xu and Ying Xia wrote the paper. All authors read and approved the final manuscript.

Funding
This work was supported by: The National Natural Science Foundation of China 81873361 (Ying Xia). The National Natural Science Foundation of China 82101533 (Yuan Xu). The National Natural Science Foundation of China 81870906 (Yilin Yang). Outstanding Talent of Changzhou "The 14th Five-Year Plan" High-Level Health Talents Training Project 2022CZZY004 (Ya Peng). Top Talent of Changzhou "The 14th Five-Year Plan" High-Level Health Talents Training Project 2022CZBJ047 (Yuan Xu).Young Talent Development Plan of Changzhou Health Commission CZQM2020043 (Yuan Xu). Science and Technology Commission of Shanghai Municipality 18401970100 (Ying Xia). Key projects of Jiangsu Commission of Health ZD2021027 (Ya Peng). Science and Technology Guide Project of Changzhou Health Commission CE20205025 (Ya Peng).

Data availability
The raw data supporting the conclusions of this manuscript will be made available in Science Data Bank with the identifier 10.57760/sciencedb.17256.

Declarations

Ethical approval
All the animal work was strictly accordance with the Chinese regulations for the administration of laboratory animals and the protocol was approved by the animal ethics committee of Changzhou First People's Hospital (approval number: 2022–015).

Consent for publication
Not applicable.

Competing interests
The authors declare no competing interests.

Author details
[1]Department of Neurosurgery, The First People's Hospital of Changzhou, Changzhou, Jiangsu, China
[2]Clinical Medical Research Center, The Third Affiliated Hospital of Soochow University, Changzhou, Jiangsu, China
[3]Shanghai Key Laboratory of Acupuncture Mechanism and Acupoint Function, Fudan University, Shanghai, China
[4]Shanghai Research Center for Acupuncture and Meridians, Shanghai, China

Received: 20 November 2024 / Accepted: 21 January 2025
Published online: 01 February 2025

References

1. Scheltens P, De Strooper B, Kivipelto M, Holstege H, Chetelat G, Teunissen CE, Cummings J, van der Flier WM. Alzheimer's disease. Lancet. 2021(10284);397:1577–90.
2. Lv B, Liang L, Chen A, Yang H, Zhang X, Guo F, Qian H. Mortality of Alzheimer's Disease and other dementias in China: past and future decades. Int J Public Health. 2023;68:1605129.
3. Jia L, Du Y, Chu L, Zhang Z, Li F, Lyu D, Li Y, Li Y, Zhu M, Jiao H, et al. Prevalence, risk factors, and management of dementia and mild cognitive impairment in adults aged 60 years or older in China: a cross-sectional study. Lancet Public Health. 2020;5(12):e661–71.
4. Bellenguez C, Kucukali F, Jansen IE, Kleineidam L, Moreno-Grau S, Amin N, Naj AC, Campos-Martin R, Grenier-Boley B, Andrade V, et al. New insights into the genetic etiology of Alzheimer's disease and related dementias. Nat Genet. 2022;54(4):412–36.
5. Torres-Berrio A, Nava-Mesa MO. The opioid system in stress-induced memory disorders: from basic mechanisms to clinical implications in post-traumatic stress disorder and Alzheimer's disease. Prog Neuropsychopharmacol Biol Psychiatry. 2019;88:327–38.
6. Babic Leko M, Hof PR, Simic G. Alterations and interactions of subcortical modulatory systems in Alzheimer's disease. Prog Brain Res. 2021;261:379–421.
7. Cai Z, Ratka A. Opioid system and Alzheimer's disease. Neuromolecular Med. 2012;14(2):91–111.
8. Hiller JM, Itzhak Y, Simon EJ. Selective changes in mu, delta and kappa opioid receptor binding in certain limbic regions of the brain in Alzheimer's disease patients. Brain Res. 1987;406(1-2):17–23.
9. Mathieu-Kia AM, Fan LQ, Kreek MJ, Simon EJ, Hiller JM. Mu-, delta- and kappa-opioid receptor populations are differentially altered in distinct areas of postmortem brains of Alzheimer's disease patients. Brain Res. 2001;893(1-2):121–34.
10. Feuerstein TJ, Gleichauf O, Peckys D, Landwehrmeyer GB, Scheremet R, Jackisch R. Opioid receptor-mediated control of acetylcholine release in human neocortex tissue. Naunyn Schmiedebergs Arch Pharmacol. 1996;354(5):586–92.

11. Xu Y, Yan J, Zhou P, Li J, Gao H, Xia Y, Wang Q. Neurotransmitter receptors and cognitive dysfunction in Alzheimer's disease and Parkinson's disease. Prog Neurobiol. 2012;97(1):1–13.
12. Ghosh S, Jana K, Wakchaure PD, Ganguly B. Revealing the cholinergic inhibition mechanism of Alzheimer's by galantamine: a metadynamics simulation study. J Biomol Struct Dyn. 2022;40(11):5100–11.
13. Aguila B, Coulbault L, Boulouard M, Leveille F, Davis A, Toth G, Borsodi A, Balboni G, Salvadori S, Jauzac P, Allouche S. In vitro and in vivo pharmacological profile of UFP-512, a novel selective delta-opioid receptor agonist; correlations between desensitization and tolerance. Br J Pharmacol. 2007;152(8):1312–24.
14. Xu Y, Zhi F, Mao J, Peng Y, Shao N, Balboni G, Yang Y, Xia Y. δ-opioid receptor activation protects against Parkinson's disease-related mitochondrial dysfunction by enhancing PINK1/Parkin-dependent mitophagy. Aging. 2020;12(24):25035–59.
15. Xu Y, Zhi F, Balboni G, Yang Y, Xia Y. Opposite roles of delta- and mu-opioid receptors in BACE1 regulation and Alzheimer's Injury. Front Cell Neurosci. 2020;14:88.
16. Martin E, El-Behi M, Fontaine B, Delarasse C. Analysis of Microglia and Monocyte-derived macrophages from the Central Nervous System by Flow Cytometry. J Vis Exp 2017;22(124):55781.
17. Xu Y, Zhi F, Peng Y, Mao J, Balboni G, Yang Y, Xia Y. A critical role of delta-opioid receptor in anti-microglial activation under stress. Front Aging Neurosci. 2022;14:847386.
18. Yang S, Zhou F, Ma M, Yuan Y, Zhao S, Yu P. Neuronostatin Promotion Soluble Aβ1-42 Oligomers: Induced Dysfunctional Brain Glucose Metabolism in Mice. Neurochem Res. 2020;45(10):2474–2486.
19. Jekabsone A, Jankeviciute S, Pampuscenko K, Borutaite V, Morkuniene R. The role of intracellular Ca2 + and mitochondrial ROS in small Aβ1–42 Oligomer-Induced Microglial Death. Int J Mol Sci 2023, 24(15):12315.
20. Wan W, Cao L, Liu L, Zhang C, Kalionis B, Tai X, Li Y, Xia S. Aβ(1–42) oligomer-induced leakage in an in vitro blood-brain barrier model is associated with up-regulation of RAGE and metalloproteinases, and down-regulation of tight junction scaffold proteins. J Neurochem. 2015;134(2):382–93.
21. Love MI, Huber W, Anders S. Moderated estimation of Fold change and dispersion for RNA-seq data with DESeq2. Genome Biol. 2014;15(12):550.
22. Xu Y, Zhi F, Shao N, Wang R, Yang Y, Xia Y. Cytoprotection against hypoxic and/or MPP(+) injury: effect of delta-opioid receptor activation on caspase 3. Int J Mol Sci 2016, 17(8):1179.
23. Cheng M, Geng Y, Chen Y, Zhang Y, Guo R, Xu H, Liang J, Xie J, Zhang Z, Tian X. delta-opioid receptor activation ameliorates lipopolysaccharide-induced inflammation and apoptosis by inhibiting the MAPK/caspase-3 pathway in BV2 microglial cells. Exp Brain Res. 2021;239(2):401–12.
24. Grigoletto J, Schechter M, Sharon R. Loss of Corticostriatal Mu-Opioid receptors in alpha-synuclein transgenic mouse brains. Life (Basel) 2022, 12(1):63.
25. Leng F, Edison P. Neuroinflammation and microglial activation in Alzheimer disease: where do we go from here? Nat Rev Neurol. 2021;17(3):157–72.
26. Norden DM, Trojanowski PJ, Villanueva E, Navarro E, Godbout JP. Sequential activation of microglia and astrocyte cytokine expression precedes increased Iba-1 or GFAP immunoreactivity following systemic immune challenge. Glia. 2016;64(2):300–16.
27. Kenkhuis B, Somarakis A, Kleindouwel LRT, van Roon-Mom WMC, Hollt T, van der Weerd L. Co-expression patterns of microglia markers Iba1, TMEM119 and P2RY12 in Alzheimer's disease. Neurobiol Dis. 2022;167:105684.
28. Siew JJ, Chen H-M, Chiu F-L, Lee C-W, Chang Y-M, Chen H-L, Nguyen TNA, Liao H-T, Liu M, Hagar H-T et al. Galectin-3 aggravates microglial activation and tau transmission in tauopathy. J Clin Investig 2024, 134(2):e165523.
29. Boza-Serrano A, Ruiz R, Sanchez-Varo R, García-Revilla J, Yang Y, Jimenez-Ferrer I, Paulus A, Wennström M, Vilalta A, Allendorf D, et al. Galectin-3, a novel endogenous TREM2 ligand, detrimentally regulates inflammatory response in Alzheimer's disease. Acta Neuropathol. 2019;138(2):251–273.
30. Puigdellívol M, Allendorf DH, Brown GC. Sialylation and Galectin-3 in microglia-mediated neuroinflammation and neurodegeneration. Front Cell Neurosci. 2020;14:162.
31. Zhang W, Chen Y, Pei H. C1q and central nervous system disorders. Front Immunol. 2023;14:1145649.
32. Hong S, Beja-Glasser VF, Nfonoyim BM, Frouin A, Li S, Ramakrishnan S, Merry KM, Shi Q, Rosenthal A, Barres BA, et al. Complement and microglia mediate early synapse loss in Alzheimer mouse models. Science. 2016;352(6286):712–6.
33. Zhang Z, Jiang J, He Y, Cai J, Xie J, Wu M, Xing M, Zhang Z, Chang H, Yu P, et al. Pregabalin mitigates microglial activation and neuronal injury by inhibiting HMGB1 signaling pathway in radiation-induced brain injury. J Neuroinflammation. 2022;19(1):231.
34. Fan H, Tang HB, Chen Z, Wang HQ, Zhang L, Jiang Y, Li T, Yang CF, Wang XY, Li X, et al. Inhibiting HMGB1-RAGE axis prevents pro-inflammatory macrophages/microglia polarization and affords neuroprotection after spinal cord injury. J Neuroinflammation. 2020;17(1):295.
35. Yang H, Wang H, Andersson U. Targeting inflammation driven by HMGB1. Front Immunol. 2020;11:484.
36. Ji H, Wang Y, Liu G, Chang L, Chen Z, Zhou D, Xu X, Cui W, Hong Q, Jiang L, et al. Elevated OPRD1 promoter methylation in Alzheimer's disease patients. PLoS ONE. 2017;12(3):e0172335.
37. Xu C, Liu G, Ji H, Chen W, Dai D, Chen Z, Zhou D, Xu L, Hu H, Cui W, et al. Elevated methylation of OPRM1 and OPRL1 genes in Alzheimer's disease. Mol Med Rep. 2018;18(5):4297–302.
38. Sarajarvi T, Marttinen M, Natunen T, Kauppinen T, Makinen P, Helisalmi S, Laitinen M, Rauramaa T, Leinonen V, Petaja-Repo U, et al. Genetic variation in delta-opioid receptor associates with increased beta- and gamma-secretase activity in the late stages of Alzheimer's Disease. J Alzheimers Dis. 2015;48(2):507–16.
39. Wang Y, Wang YX, Liu T, Law PY, Loh HH, Qiu Y, Chen HZ. Mu-opioid receptor attenuates Abeta oligomers-induced neurotoxicity through mTOR signaling. CNS Neurosci Ther. 2015;21(1):8–14.
40. Teng L, Zhao J, Wang F, Ma L, Pei G. A GPCR/secretase complex regulates beta- and gamma-secretase specificity for abeta production and contributes to AD pathogenesis. Cell Res. 2010;20(2):138–53.
41. Min J-W, Liu Y, Wang D, Qiao F, Wang H. The non-peptidic δ-opioid receptor agonist Tan-67 mediates neuroprotection post-ischemically and is associated with altered amyloid precursor protein expression, maturation and processing in mice. J Neurochem. 2018;144(3):336–47.
42. Pluta R. Alzheimer's Disease Connected Genes in the Post-Ischemic Hippocampus and Temporal Cortex. Genes (Basel) 2022, 13(6):1059.
43. Zhang J, Yin DP, Zhang Y, Zhang JN, Yang Y, Zhang ZQ, Zhou L, Lv Y, Huang HW, Cao C. Identification of Galphai3 as a novel molecular therapeutic target of cervical cancer. Int J Biol Sci. 2022;18(15):5667–80.
44. Zhang R, Xue G, Wang S, Zhang L, Shi C, Xie X. Novel object recognition as a facile behavior test for evaluating drug effects in AbetaPP/PS1 Alzheimer's disease mouse model. J Alzheimers Dis. 2012;31(4):801–12.
45. Tanguturi P, Streicher JM. The role of opioid receptors in modulating Alzheimer's Disease. Front Pharmacol. 2023;14:1056402.
46. O'Leary TP, Brown RE. Visuo-spatial learning and memory deficits on the Barnes maze in the 16-month-old APPswe/PS1dE9 mouse model of Alzheimer's disease. Behav Brain Res. 2009;201(1):120–7.
47. Jankowsky JL, Melnikova T, Fadale DJ, Xu GM, Slunt HH, Gonzales V, Younkin LH, Younkin SG, Borchelt DR, Savonenko AV. Environmental enrichment mitigates cognitive deficits in a mouse model of Alzheimer's disease. J Neurosci. 2005;25(2):5217–24.
48. Roy ER, Chiu G, Li S, Propson NE, Kanchi R, Wang B, Coarfa C, Zheng H, Cao W. Concerted type I interferon signaling in microglia and neural cells promotes memory impairment associated with amyloid beta plaques. Immunity. 2022;55(5):879–e894876.
49. Zhao N, Qiao W, Li F, Ren Y, Zheng J, Martens YA, Wang X, Li L, Liu CC, Chen K et al. Elevating microglia TREM2 reduces amyloid seeding and suppresses disease-associated microglia. J Exp Med 2022, 219(12):e20212479.
50. Bartels T, De Schepper S, Hong S. Microglia modulate neurodegeneration in Alzheimer's and Parkinson's diseases. Science. 2020;370(6512):66–9.
51. Naj AC, Jun G, Reitz C, Kunkle BW, Perry W, Park YS, Beecham GW, Rajbhandary RA, Hamilton-Nelson KL, Wang LS, et al. Effects of multiple genetic loci on age at onset in late-onset Alzheimer disease: a genome-wide association study. JAMA Neurol. 2014;71(11):1394–404.
52. Ting SM, Zhao X, Zheng X, Aronowski J. Excitatory pathway engaging glutamate, calcineurin, and NFAT upregulates IL-4 in ischemic neurons to polarize microglia. J Cereb Blood Flow Metab. 2020;40(3):513–27.
53. Borst K, Dumas AA, Prinz M. Microglia. Immune and non-immune functions. Immunity. 2021;54(10):2194–208.
54. Dejanovic B, Wu T, Tsai MC, Graykowski D, Gandham VD, Rose CM, Bakalarski CE, Ngu H, Wang Y, Pandey S, et al. Complement C1q-dependent excitatory and inhibitory synapse elimination by astrocytes and microglia in Alzheimer's disease mouse models. Nat Aging. 2022;2(9):837–50.
55. Ding Y, Li J, Lai Q, Azam S, Rafols JA, Diaz FG. Functional improvement after motor training is correlated with synaptic plasticity in rat thalamus. Neurol Res. 2002;24(8):829–36.

56. Sasaki T, Liu K, Agari T, Yasuhara T, Morimoto J, Okazaki M, Takeuchi H, Toyoshima A, Sasada S, Shinko A, et al. Anti-high mobility group box 1 antibody exerts neuroprotection in a rat model of Parkinson's disease. Exp Neurol. 2016;275 Pt 1:220–31.
57. Xiong X, Gu L, Wang Y, Luo Y, Zhang H, Lee J, Krams S, Zhu S, Zhao H. Glycyrrhizin protects against focal cerebral ischemia via inhibition of T cell activity and HMGB1-mediated mechanisms. J Neuroinflammation. 2016;13(1):241.
58. Tanaka H, Homma H, Fujita K, Kondo K, Yamada S, Jin X, Waragai M, Ohtomo G, Iwata A, Tagawa K, et al. YAP-dependent necrosis occurs in early stages of Alzheimer's disease and regulates mouse model pathology. Nat Commun. 2020;11(1):507.
59. Gao JM, Zhang X, Shu GT, Chen NN, Zhang JY, Xu F, Li F, Liu YG, Wei Y, He YQ, et al. Trilobatin rescues cognitive impairment of Alzheimer's disease by targeting HMGB1 through mediating SIRT3/SOD2 signaling pathway. Acta Pharmacol Sin. 2022;43(10):2482–94.
60. Gaikwad S, Puangmalai N, Bittar A, Montalbano M, Garcia S, McAllen S, Bhatt N, Sonawane M, Sengupta U, Kayed R. Tau oligomer induced HMGB1 release contributes to cellular senescence and neuropathology linked to Alzheimer's disease and frontotemporal dementia. Cell Rep. 2021;36(3):109419.
61. Zwagerman N, Plumlee C, Guthikonda M, Ding Y. Toll-like receptor-4 and cytokine cascade in stroke after exercise. Neurol Res. 2010;32(2):123–6.
62. Mein N, von Stackelberg N, Wickel J, Geis C, Chung HY. Low-dose PLX5622 treatment prevents neuroinflammatory and neurocognitive sequelae after sepsis. J Neuroinflammation. 2023;20(1):289.

Publisher's note